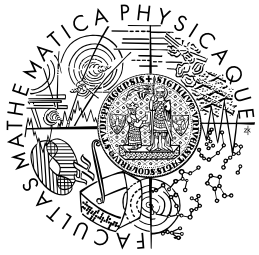

FACULTY
OF MATHEMATICS
AND PHYSICS
Charles University

BACHELOR THESIS

Matúš Rojik

Modeling atomic nuclei using supercomputers for precision tests of the Standard model

Institute of Particle and Nuclear Physics

Supervisor of the bachelor thesis: Ing. Tomáš Dytrych, Ph.D.

Study programme: Physics

Study branch: FP

Prague 2023

I declare that I carried out this bachelor thesis independently, and only with the cited sources, literature and other professional sources. It has not been used to obtain another or the same degree.

I understand that my work relates to the rights and obligations under the Act No. 121/2000 Sb., the Copyright Act, as amended, in particular the fact that the Charles University has the right to conclude a license agreement on the use of this work as a school work pursuant to Section 60 subsection 1 of the Copyright Act.

In ..... date ....

Author's signature

I would like to thank my supervisor, Ing. Tomáš Dytrych Ph.D., for guiding me through the work on my thesis, for his patience, and for his willingness to always meet up and discuss any problems or questions I had.

I would like to thank my parents, for their endless and unconditional support.

Title: Modeling atomic nuclei using supercomputers for precision tests of the Standard model

Author: Matúš Rojik

Institute: Institute of Particle and Nuclear Physics

Supervisor: Ing. Tomáš Dytrych, Ph.D., Nuclear Physics Institute, CAS, Řež

Abstract: One of the most important problems of modern theoretical nuclear physics is to accurately determine the structure of atomic nuclei. To obtain results that are in agreement with experimental data, one needs to solve the nuclear many-body problem with high enough precision. Ab initio methods address this problem by trying to solve the emergent Schrödinger equation for all nucleons with a realistic interaction. Until recently, they were applicable only to light nuclei because of the high computational demands. In this work, we briefly present the theory behind the symmetry-adapted no-core shell model, which allows for truncation of the model space based on innate symmetry of nuclei that leads to reduction of the Hamiltonian matrix dimensions, while the convergence of the full space is conserved. We explore its predictive power by studying beta decays of various nuclei and discuss possible applications of the symmetry-adapted no-core shell model for the study of physics beyond the Standard Model.

Keywords: Ab initio calculations, Symmetry-adapted no-core shell model , Beta decay, Physics beyond the Standard Model

Contents

Introduction

At energies small enough compared to the masses of particles that mediate nuclear forces, the nucleus can be looked upon as a self-bound many-body system made up of nucleons. The nucleus has two types of degrees of freedom - collective, which describe the state of the nucleus as a whole, and intrinsic, which describe the state of individual nucleons. An accurate theoretical description of the structure of atomic nuclei and their properties poses a difficult problem since one needs to take both their microscopic and collective nature into account. Moreover, the interactions between nucleons are far from well-understood. Various models have been developed to describe and capture the complex nature of the nucleus, taking different approaches to this problem.

We begin this work by describing the nuclear shell model with a core. This model assumes that nucleons occupy certain levels that are ordered by increasing energy, analogous to the idea of atomic orbitals. According to this model, only the protons and neutrons in the valence shell interact through nuclear interactions and the rest moves in a mean-field potential.

The no-core nuclear shell model makes no apriori assumptions about the nuclear structure and tries to solve the corresponding Schrödinger equation ab initio - from first principles. In this case, that means that all nucleons, not only the ones in the valence shell, interact with each other through realistic many-body interactions derived from effective field theories. The main disadvantage of this approach is the immensely large dimensions of the Hamiltonian matrix that needs to be diagonalized. Even with the use of powerful modern supercomputers, medium-mass and heavier nuclei are out of reach.

By exploiting the SU(3) group symmetry, that was first applied in nuclear physics by Elliott [1], a basis that takes the collective nature of nuclei into account can be constructed. The symmetry-adapted no-core shell model adapts this basis with great success allowing us to study the shapes of nuclei from first principles. Furthermore, the advantageous structure of the SU(3) basis can be used to reduce the dimensions of no-core shell model calculations.

The focus of our work is to study possible applications of the symmetry-adapted no-core shell model for electroweak processes in nuclei, i.e., β-decay transitions. An accurate theoretical treatment of β-decay is especially important since it can be used to look for physics beyond the standard model. Some of the ways ab initio calculations can be utilized to probe new physics are outlined in the second chapter, along with the theory behind β-decay. In the last chapter, we report the results of our findings for nuclei with mass $A \leq 16$.

1. The Nuclear Shell Model

1.1 The Core Shell Model

The Hamiltonian of the nuclear many-body problem for A nucleons can be formulated as

$$H = \sum_{i=1}^{A} T_i + \tfrac{1}{2} \sum_{i,j=1}^{A} V_{i,j}, \tag{1.1.1}$$

where T_i is the kinetic energy of the individual nucleon and $V_{i,j}$ is a two-body interaction. By adding and subtracting a summed single-particle potential, we can rewrite the Hamiltonian as

$$H = \left[\sum_{i=1}^{A} T(\boldsymbol{r}_i) + U(\boldsymbol{r}_i)\right] + \left[\tfrac{1}{2} \sum_{i,j=1}^{A} V(\boldsymbol{r}_i, \boldsymbol{r}_j) - \sum_{i=1}^{A} U(\boldsymbol{r}_i)\right] \equiv H_{\text{mf}} + H_{\text{res}}, \tag{1.1.2}$$

where $\boldsymbol{r}_i$ denotes the position and any other degree of freedom of a nucleon. The first term of (1.1.2) is known as the mean-field Hamiltonian

$$H_{\text{mf}} = \sum_{i=1}^{A} T(\boldsymbol{r}_i) + U(\boldsymbol{r}_i) \equiv \sum_{i=1}^{A} h_0(\boldsymbol{r}_i) \tag{1.1.3}$$

which describes the movement of each nucleon in an average, mean-field potential $U(\boldsymbol{r}_i)$ that is generated by all other nucleons. In the mean-field approximation, it is therefore assumed that the nucleons do not interact with each other. The second term is known as the residual interaction

$$H_{\text{res}} = \tfrac{1}{2} \sum_{i,j=1}^{A} V(\boldsymbol{r}_i, \boldsymbol{r}_j) - \sum_{i=1}^{A} U(\boldsymbol{r}_i) \tag{1.1.4}$$

and describes the remaining two-body interaction.

We will first solve the non-relativistic Schrödinger equation $H|\psi\rangle = E|\psi\rangle$ with the mean-field Hamiltonian (1.1.3). Since the nucleons do not interact we can substitute a wavefunction in the separated form

$$\psi(\boldsymbol{r}_1, \boldsymbol{r}_2, ..., \boldsymbol{r}_A) = \phi_1(\boldsymbol{r}_1)\phi_2(\boldsymbol{r}_2)...\phi_A(\boldsymbol{r}_A), \tag{1.1.5}$$

where the function ϕ_i is the eigenfunction of the single-particle Hamiltonian

$$h_0(\boldsymbol{r})\phi_i(\boldsymbol{r}) = \epsilon_i \phi_i(\boldsymbol{r}). \tag{1.1.6}$$

By substituing (1.1.6) into the original Schrödinger equation we obtain an expression for the total energy of a nucleus

$$E = \sum_{i=1}^{A} \epsilon_i. \tag{1.1.7}$$

Since the nucleus is a fermionic system, its wavefunction needs to satisfy the Pauli exclusion principle, which (1.1.5) does not. We usually construct the A-nucleon wavefunction in the form of a Slater determinant

$$\psi(\boldsymbol{r}_1, \boldsymbol{r}_2, ..., \boldsymbol{r}_A) = \frac{1}{\sqrt{A!}} \begin{vmatrix} \phi_1(\boldsymbol{r}_1) & \phi_1(\boldsymbol{r}_2) & \cdots & \phi_1(\boldsymbol{r}_A) \\ \phi_2(\boldsymbol{r}_1) & \phi_2(\boldsymbol{r}_2) & \cdots & \phi_2(\boldsymbol{r}_A) \\ \phi_3(\boldsymbol{r}_1) & \phi_3(\boldsymbol{r}_2) & \cdots & \phi_3(\boldsymbol{r}_A) \\ \vdots & \vdots & \ddots & \vdots \\ \phi_A(\boldsymbol{r}_1) & \phi_A(\boldsymbol{r}_2) & \cdots & \phi_A(\boldsymbol{r}_A) \end{vmatrix} \tag{1.1.8}$$

which conforms to the Pauli exclusion principle by definition.

The problem that remains is then the choice of an optimal mean-field potential that describes the nuclear structure as best as possible and minimizes the residual interaction. This can be treated as a variational problem where one tries to find single-particle states ϕ_i that minimize the ground-state energy. However, this process is often skipped, and a phenomenological potential, such as Woods-Saxon

$$U_{\mathrm{WS}}(r) = -\frac{V_0}{1 + \mathrm{e}^{(r-R)/a}} \tag{1.1.9}$$

or harmonic oscillator (HO)

$$U_{\mathrm{HO}}(r) = \tfrac{1}{2} m_n \omega^2 r^2 \tag{1.1.10}$$

is chosen instead. These potentials are central, i.e., depend only on r.

It turns out that some experimental results can be reproduced with just the mean-field Hamiltonian and without taking the residual interaction into consideration. This approach is also known as the *independent particle model*. We assume that the mean-field $U(r)$ is described well enough by the HO potential and the single-particle Hamiltonian in (1.1.3) is then

$$h_0 = -\frac{\hbar^2}{2m_n}\Delta + \tfrac{1}{2} m_n \omega^2 r^2. \tag{1.1.11}$$

We further modify this Hamiltonian by adding an additional term proportional to the product of angular momentum $\boldsymbol{l}$ and spin $\boldsymbol{s}$ and a term proportional to $\boldsymbol{l}^2$

$$h = h_0 + a\boldsymbol{l}\cdot\boldsymbol{s} + b\boldsymbol{l}^2. \tag{1.1.12}$$

Solving the Schrödinger equation with the modified Hamiltonian (1.1.12) yields single-particle wavefunctions that correctly predict the so-called magic numbers - proton (Z) and neutron (N) numbers of stable configurations that correspond to filled nuclear shells (Fig. 1.1). The consequences of the inclusion of spin-orbit interaction term $\boldsymbol{l}\cdot\boldsymbol{s}$ in the single-particle Hamiltonian were first described by M. G. Mayer in 1949 in her pioneering work [2]. The term $\boldsymbol{l}^2$ does not have an effect on the magic numbers but needs to be included to reproduce the correct ordering of energy shells (Fig 1.1).

Exact diagonalization of the nuclear Hamiltonian (1.1.2) is a computationally intensive task. To make this problem more manageable, the concept of an inert core, which consists of non-interacting nucleons that occupy single-particle states of the mean-field potential, is introduced. The idea is then to choose a *model space* that is made up of only a few orbits around the Fermi energy, which is the energy level that divides the empty orbitals and the last occupied shell. The nucleons that occupy this shell are considered active and interact through the two- or more-body residual interaction. These nucleons can be excited above the Fermi level to a higher shell that is included in the valence (or model) space creating a hole in the valence shell. In this way, we have excluded the lowest states from our calculations, which became a part of the inert core, as well as the highly excited states above the Fermi energy, because we are usually interested only in the low-lying states that are well-described by excitations around the Fermi level. Naturally, the higher the excitations we want to consider, the larger

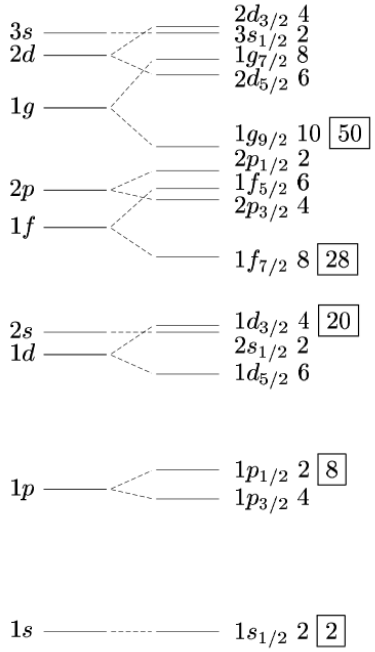

Figure 1.1: Degenerate energy spectrum one obtains by solving the Schrödinger equation with the Hamiltonian (1.1.12). The nuclear shell states are ordered by increasing energy and labeled using the radial ($n_r = (n - l + 2)/2$), orbital (l), and total angular momentum ($j = l \pm \frac{1}{2}$) oscillator quantum numbers: $n_r l_j = 1s_{1/2}$, $1p_{3/2}$, $1p_{1/2}$, ... The numbers in the boxes on the right side of the figure represent the magic numbers.

must be our model space. This approach is known as the *interacting shell model* or *valence configuration interaction* [3, 4, 5].

In the recent two decades, ab initio methods that try to solve the Schrödinger equation with realistic two- and three-body interactions for all nucleons have gained immense popularity [6]. One of such methods, the no-core shell model (NCSM) [7] and its extension, the symmetry-adapted no-core shell model (SA-NCSM) [8], will be described in the following sections.

1.2 The No-Core Shell Model

As we have already alluded to, NCSM seeks to describe the atomic nucleus from first principles. It assumes that all nucleons are active and the interactions between them are realistic, described by two-, three- (or more) body potentials that emerge from effective field theories. The starting Hamiltonian of our A-nucleon problem is

$$H = \frac{1}{A}\sum_{i<j}^{A}\frac{(\boldsymbol{p}_i - \boldsymbol{p}_j)^2}{m_n} + \sum_{i<j}^{A} V_{\mathrm{NN},ij} + \sum_{i<j<k}^{A} V_{\mathrm{NNN},ijk} + ..., \tag{1.2.1}$$

where V_{NN} is a two nucleon interaction, V_{NNN} a three nucleon one. In general, interactions between more than three nucleons can be considered. Note that this Hamiltonian is translationally invariant.

Similarly to traditional shell model calculations, solving the Schrödinger equation in the full, infinite-dimensional Hilbert space is not feasible, and therefore we must limit ourselves to only a finite part of it by choosing a suitable model space. This is then reflected in the choice of a finite basis. The Schrödinger equation $H|\psi\rangle = E|\psi\rangle$ is transformed into an eigenvalue problem

$$\sum_j H_{ij} c_j = E c_i, \tag{1.2.2}$$

where c_i are the expansion coefficients of state $\psi = \sum_i c_i \psi_i$ in the orthonormal basis $\{\psi_i\}$ and $H_{ij} = \langle \psi_i | H | \psi_j \rangle$ are the Hamiltonian matrix elements. The eigenvalues and eigenvectors are then found by diagonalizing the matrix H_{ij}; in shell model calculations, the Lanczos algorithm [9] is usually employed to solve this problem.

In the standard shell model, we have limited our model space to only a few shells around the Fermi energy. In NCSM calculations, a finite HO basis is used, and the model space is truncated from above by the parameter $\mathrm{N_{totmax}}$, which is the sum of all HO excitations. The highly excited states remain excluded to make the calculations manageable.

Usually, a different parameter $\mathrm{N_{max}}$, which has the following meaning, is introduced. Let us suppose that the nucleons do not interact. In that case, they fill the nuclear shells in accordance with the Pauli exclusion principle and form an unperturbed ground state (GS) in which none of the nucleons are excited. The number of HO quanta that represent such a state is equal to $\sum_{i=1}^{A} n_i = N_0 \leq \mathrm{N_{totmax}}$. The parameter $\mathrm{N_{max}}$ then represents the amount of HO excitation energy quanta that are available to nucleons above the GS, $\mathrm{N_{max}} = \mathrm{N_{totmax}} - N_0$. A model space truncated by $\mathrm{N_{max}}$ contains configurations that carry all posible excitation quanta lower or equal to $\mathrm{N_{max}}$. A space containing configurations that carry equal amount of excitation quanta will be denoted by $N\hbar\Omega$, i.e., a configuration space characterized by $2\hbar\Omega$ contains all configuration that carry two excitation quanta. Since the parity of the wavefunction must be conserved, for every value $\mathrm{N_{max}}$ we consider only even or odd $\mathrm{N}\hbar\Omega$ subspaces, i.e., the only possible subspaces are $\mathrm{N_{max}}\hbar\Omega$, $(\mathrm{N_{max}} - 2)\hbar\Omega$, $(\mathrm{N_{max}} - 4)\hbar\Omega$, ..., $1\hbar\Omega$ or $0\hbar\Omega$.

For nuclei with $A \leq 4$, $\mathrm{N_{max}} = \mathrm{N_{totmax}}$ since the nucleons fill only one shell, the s-shell. For p-shell and higher nuclei, these parameters differ. As an example, let us take the nucleus ^{12}C, which has the s-shell completely filled with 2 protons and 2 neutrons, and its p-shell is occupied by the remaining 8 nucleons (Fig. 1.2). Therefore, there needs to be atleast $N_0 = 8$ HO quanta to describe the ^{12}C GS and $\mathrm{N_{max}} = \mathrm{N_{totmax}} - 8$. Let us now suppose we have a model space defined by $N_{\mathrm{max}} = 2$, i.e., there is a maximum of two excitation energy quanta available. They can either excite the p-shell nucleons, moving one of them from the p-shell to the pf-shell or two of them to the sd-shell or excite the s-shell nucleons, moving one of them sd-shell or two of them to the p-shell.

1.2.1 The Basis of NCSM

In this section, we discuss the HO basis and different coupling schemes that are employed in NCSM calculations. One of the problems one faces when trying to expand the many-body wavefunction into a HO basis is the choice of the

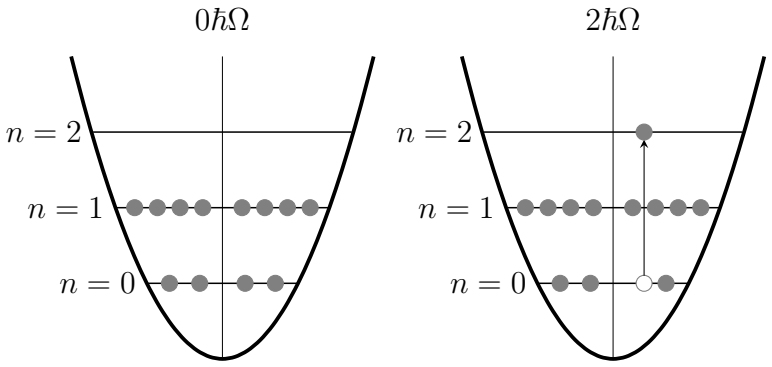

Figure 1.2: Left: The ground state of ^{12}C. Right: One of the possible $2\hbar\Omega$ configurations of ^{12}C.

correct coordinates. One can either work with the Jacobi coordinates, which are defined relative to the center of mass, or with single-particle coordinates, which are defined relative to a single point in space. The former does not contain center of mass motion, but antisymmetrization is difficult. Single-particle states are easy to antisymmetrize but contain unwanted center of mass motion [7]. In the following text, we use single-particle states and deal with the factorization of the center of mass motion in section 1.2.2.

Single-Particle Harmonic Oscillator States

In the HO basis, the wavefunction of a single particle with spin $\boldsymbol{\sigma}$ and isospin $\boldsymbol{\tau}$ can be expressed in the form

$$\phi_{nljm_jm_t}(\boldsymbol{r},\boldsymbol{\sigma},\boldsymbol{\tau},b) = R_{nl}(r,b)\left[Y_l\left(\frac{\boldsymbol{r}}{r}\right)\times\chi(\boldsymbol{\sigma})_s\right]^j_{m_j}\chi(\boldsymbol{\tau})_{tm_t}, \tag{1.2.3}$$

where R_{nl} describes the radial part of the wavefunction and Y_{lm} is a spherical harmonic that describes the angular dependence. These two functions are obtained by solving the Schrödinger equation with an isotropic HO potential (1.1.10). The remaining terms $\chi(\boldsymbol{\tau})_{tm_t}$ and $\chi(\boldsymbol{\sigma})_{sm_s}$ are two-dimensional state vectors that describe the spin and isospin degrees of freedom. The labels s and t are superfluous since they are always equal to 1/2 for nucleons and consequently $m_s, m_t = \pm\frac{1}{2}$. Sometimes, protons and neutrons are treated as separate particles, and the isospin degree of freedom is not needed. Furthermore, in (1.2.3) we have coupled the angular momentum l and spin s into the total momentum j, where $[Y_l\times\chi_s]^j_{m_j}$ is the tensor product

$$\left[Y_l\left(\frac{\boldsymbol{r}}{r}\right)\times\chi(\boldsymbol{\sigma})_s\right]^j_{m_j} = \sum_{m\,m_s}\langle l\,\tfrac{1}{2}\,m\,m_s|jm_j\rangle Y_{lm}\chi_{1/2m_s} \tag{1.2.4}$$

The parameter b is the oscillator length and its relationship to HO frequency is given by

$$b = \sqrt{\frac{\hbar}{m_n\Omega}}. \tag{1.2.5}$$

For the value typically used in NCSM calculations, $\hbar\Omega = 20$ MeV, the oscillator length is equal to $b = 1.44$ fm.

The M-scheme

From the single-particle states (1.2.3) antisymmetrized wavefunctions in the form of Slater determinants (1.1.8) can be constructed. A basis made up of Slater determinants is known as the Glasgow M-scheme basis [10]. The values of the total momentum and total isospin projection quantum numbers $M_J = \sum_i m_{j,i}$ and $M_T = \frac{1}{2}(Z - N)$ are good quantum numbers in this basis. One of the advantages of this basis is that we do not have to deal with complicated couplings of momenta, which is unavoidable when constructing a basis with J as a good quantum number.

For a nucleus with $J = 0$, the model space is comprised of Slater determinants with $M_J = 0$, since that is the only possible projection value. When we wish to describe a nucleus with a higher value of J, we can choose to construct a basis from determinants with any of the $2J+1$ possible M_J values. For example, when describing a nucleus with $J = 2$ the optimal choice would be $M_J = 2$, since this choice excludes states with $J = 0$ and $J = 1$ and leads to the smallest dimension of the basis.

The construction of an M-scheme basis can be easily understood using a simple example. Let us suppose that we want to create an M-scheme basis for ${}^{6}_{3}\mathrm{Li}$ and our model space is defined by $\mathrm{N_{max}} = 0$. The s-shell is filled completely by 2 protons and 2 neutrons. One neutron and one proton are left over and must occupy a state in the $\mathrm{p}_{3/2}$ or $\mathrm{p}_{1/2}$ shell, there are therefore 6 available states for each. Next, let us choose M_J to be equal to 0. Constrained by this condition and taking the Pauli exclusion principle into account there 10 possible ways to arrange the nucleons left - the dimension of our basis is 10.

Another major advantage of the M-scheme is that occupation number representation can be utilized with great efficiency. A Slater determinant in second-quantized form can be expressed as

$$a^{\dagger}_{n_1 l_1 j_1 m_{j_1} m_{t_1}} ... a^{\dagger}_{n_A l_A j_A m_{j_A} m_{t_A}} |0\rangle, \tag{1.2.6}$$

where $a^{\dagger}_{nljm_j m_t}$ is a particle creation operator that creates a nucleon in state specified by the n, l, j, m_j, m_t quantum numbers and $|0\rangle$ is the particle vacuum. We can then assign a single bit to represent an occupied or an empty state (1 or 0). Using this approach, even an M-scheme basis of considerable dimension can be stored efficiently in computer memory.

In modern NCSM calculations, the M-schceme basis is largely preferred due to its computational advantages. The dimension of the M-scheme basis is typically large, but the Hamiltonian matrix is sparse and its matrix elements can be quickly evaluated using bit operations.

The J-scheme

Another option is to construct a basis by coupling momenta of individual single-particle states to a total angular momentum number J, the so-called $J-$scheme. For example, a two-particle state in the J-scheme is constructed as

$$\left(a^{\dagger}_{nljm_t} \times a^{\dagger}_{n'l'j'm'_t}\right)^{JM_J} |0\rangle = \sum_{m_j m'_j} \langle jj' m_j m'_j | JM_J \rangle a^{\dagger}_{nljm_j m_t} a^{\dagger}_{n'l'j'm'_j m'_t} |0\rangle. \tag{1.2.7}$$

The two-particle state (1.2.7) can be generalized for A nucleons by coupling additional momenta. Sometimes, when the isospin symmetry-breaking due to the Coulomb force is ignored, the isospins are also coupled into total isospin T and its projection M_T. The Hamiltonian in J-scheme basis is block-diagonal in J (or in J, T) and calculations for concrete values of J can be performed within a single block. The dimensions of the Hamiltonian matrix are therefore smaller in the J-coupled basis. However, the matrixes are denser, and evaluation is slower. Another advantage of the J-scheme compared to the M-schceme is the fact that since J is not a good quantum number in the latter, it can lead to complications when evaluating matrix elements of operators.

1.2.2 Spurious States and the Center of Mass

Constructing a basis from single particle states violates the translational invariance of the Hamiltonian since by using single particle coordinates $\boldsymbol{r}_i$ we have defined a unique point in space, from which all positions and momenta originate. This leads to creation of states which are excited with respect to the center of mass [11]. However, in a HO basis with the $\mathrm{N_{max}}$ truncation, this problem can be treated since this basis allows for exact factorization of motion of the center of mass.

The center-of-mass motion can be described by the Hamiltionan

$$H_{\mathrm{cm}} = \frac{\boldsymbol{P}^2}{2m_n A} + \frac{1}{2} m_n A \Omega^2 \boldsymbol{R}^2. \tag{1.2.8}$$

Here, $\boldsymbol{R} = \frac{1}{A}\sum_{i=1}^{A} \boldsymbol{r_i}$ and $\boldsymbol{P}$ is the center-of-mass momentum. The center-of-mass states are then classified by the major oscillator quantum number N_{cm}, and they form a spectrum with energies $E_{\mathrm{cm}} = \hbar\Omega(N_{\mathrm{cm}} + 3/2)$. The complete Hamiltonian can be written as

$$H = H_{\mathrm{int}} + H_{\mathrm{cm}}, \tag{1.2.9}$$

where H_{int} is the transliationally invariant Hamiltonian (1.2.1). The many-body wavefunctions expanded in the Slater determinant basis can then be decomposed into two parts

$$\psi(\boldsymbol{r}_1, \boldsymbol{r}_2, ..., \boldsymbol{r}_A) = \psi_{\mathrm{int}}(\boldsymbol{\xi}_1, \boldsymbol{\xi}_2, ..., \boldsymbol{\xi}_{A-1}) \otimes \phi_{\mathrm{cm}}(\boldsymbol{R}), \tag{1.2.10}$$

a part that describes the center of mass ϕ_{cm}, which is the eigenfunction of H_{cm}, and an intrinsic part ψ_{int}, the eigenfunction of H_{int}, that describes the many-body wavefunction in coordinates relative to the center of mass, the Jacobi coordinates. This decomposition is possible only in the HO basis [7]. For an A-particle system, these coordinates are defined as

$$\boldsymbol{\xi}_0 = \sqrt{\frac{1}{A}} \left[\boldsymbol{r}_1 + \boldsymbol{r}_2 + ... + \boldsymbol{r}_A\right] \tag{1.2.11}$$

$$\boldsymbol{\xi}_1 = \sqrt{\frac{1}{2}} \left[\boldsymbol{r}_1 - \boldsymbol{r}_2\right] \tag{1.2.12}$$

$$\boldsymbol{\xi}_2 = \sqrt{\frac{2}{3}} \left[\frac{1}{2}(\boldsymbol{r}_1 + \boldsymbol{r}_2) - \boldsymbol{r}_3\right] \tag{1.2.13}$$

$$\vdots$$

$$\boldsymbol{\xi}_{A-1} = \sqrt{\frac{A-1}{A}}\left[\frac{1}{A-1}(\boldsymbol{r}_1 + \boldsymbol{r}_2 + ... + \boldsymbol{r}_{A-1}) - \boldsymbol{r}_A\right], \tag{1.2.14}$$

where the zeroth Jacobi coordinate is proportional to the position of the center of mass, since $\boldsymbol{\xi}_0 = \sqrt{A}\boldsymbol{R}$.

The states with $N_{cm} > 0$ are referred to as spurious and it needs to be assured that they do not mix with 'good' states that have $N_{cm} = 0$. This issue is treated by utilizing the Gloeckner-Lawson projection method [12], which solves this problem without the need for a change of basis. The basic procedure is as follows.

The Schrödinger equation is solved with the modified Hamiltonian

$$H = H_{\text{int}} + \beta\left(H_{\text{cm}} - \frac{3}{2}\hbar\Omega\right), \tag{1.2.15}$$

where depending on the value of β[1], the spurious states are shifted upwards in the spectrum, and the energies of good states are unchanged, as $\left(H_{\text{cm}} - \frac{3}{2}\hbar\Omega\right)\phi_{\text{cm}} = 0$ for $N_{\text{cm}} = 0$.

1.2.3 Nuclear Interactions

The recent success of ab initio methods can in part be attributed to the progress made in the construction of realistic nuclear potentials in recent decades. The fundamental interactions between quarks and gluons are described by the theory of quantum chromodynanmics (QCD). However, in the low energy spectrum, which is the main interest of nuclear physics, QCD is non-perturbative. This fact makes the description of even light nuclei at the QCD level very difficult.

The gap between the fundamental level of quarks, gluons, and nucleons is bridged by the effective field theory (EFT). In the framework of EFT, one can construct interactions that are consistent with the symmetries of QCD and that are expanded in terms of (Q/Λ), where Q is the typical value of momenta of the system we want to capture and $\Lambda \approx 1$ GeV represents values of momenta at which the theory breaks down. Nuclear interactions cannot be derived completely from theoretical models. They are parametrized by low energy constants that are determined by fits to experimental data [6].

In the third chapter, we use the potential NNLO_{opt} [13], which optimizes the nuclear force at the next-to-next-to-leading order of EFT at which three-body forces emerge (Fig. 1.3). The nucleon force of NNLO_{opt} is adjusted to the binding energies of $A = 3$ and 4 nuclei.

We also employ the JISP16 [14] potential. The JISP family of potentials is based on the J-matrix inverse scattering approach, which is used to derive the inter-nucleon forces. The two-nucleon JISP16 interaction was fitted to reproduce the binding energies of nucleons with masses $A \leq 16$.

To perform ab initio studies of heavier nuclei, the basis size has to be expanded correspondingly, which unavoidably means that highly excited HO states are included, and the spatial resolution of our wavefunctions is greater. This leads to the fact that the inter-nucleon interaction is probed at shorter distances where

[1] We use the value $\beta = 20$ in our calculations. Generally, any 'large-enough' value is sufficient

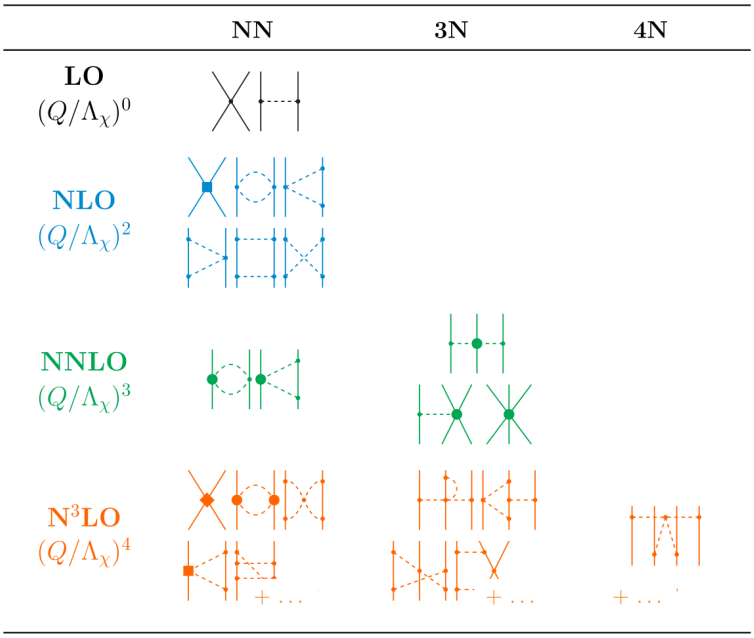

Figure 1.3: Pertubation orders of the chiral (i.e. pionful) EFT. Dashed lines represent exchanges of pions, solid dots represents low-energy constants. Figure adapted from [6].

it has a strongly repulsive core, and we have to deal with higher momenta, which are not treated well by our low-energy approach. This problem is especially relevant for potentials that emerge from EFT ('hard-core potentials'), and different renormalization techniques that supress or decouple high momentum terms [7, 5] have to be employed. The JISP16 is a soft-core potential, and it has been shown that it provides good predictions even without renormalization [14].

1.3 Convergence and Extrapolations

In the NCSM we limit our calculations to only a part of the full Hilbert space. The size of our basis is limited by the N_{max} cut-off, as was discussed earlier. Moreover, our basis depends on the HO frequency $\hbar\Omega$. It follows that energies or operator matrix elements calculated within the NCSM framework will also depend on these parameters. However, as we expand the size of our model space, it is reasonable to expect that the calculated values of operator matrix elements will converge to the 'true' values one would obtain by solving the Schrödinger equation in infinite-dimensional space. In practice, we are limited by computing resources and reasonably good convergence can be achieved only for light nuclei. In order to obtain meaningful values from the NCSM framework, various techniques that extrapolate results from limited model spaces and give reasonable estimates of their errors have to be employed. Some of these techniques will be described in this section.

A typical dependence of ground state energy on (N_{max}, $\hbar\Omega$) is shown on figure 1.4. The extrapolation techniques described in [15] exploit the fact that the convergence appears to be monotonous and one can identify a minimum with respect to $\hbar\Omega$ at each and every value of N_{max}. The general procedure is to first

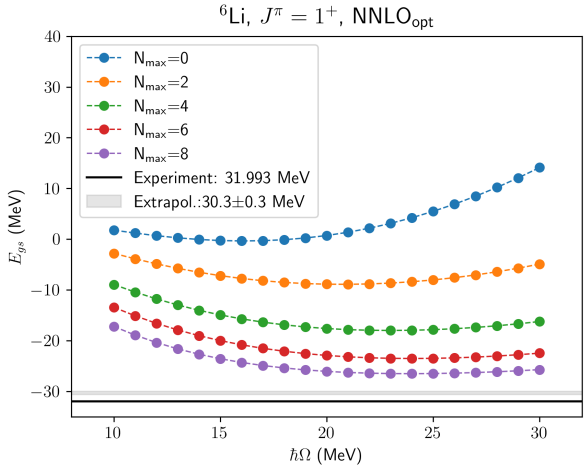

Figure 1.4: Convergence of the binding energy of the ground state of ^{6}Li, $J^\pi = 1^+$ and the extrapolated value, calculated with the NNLO$_{\text{opt}}$ potential

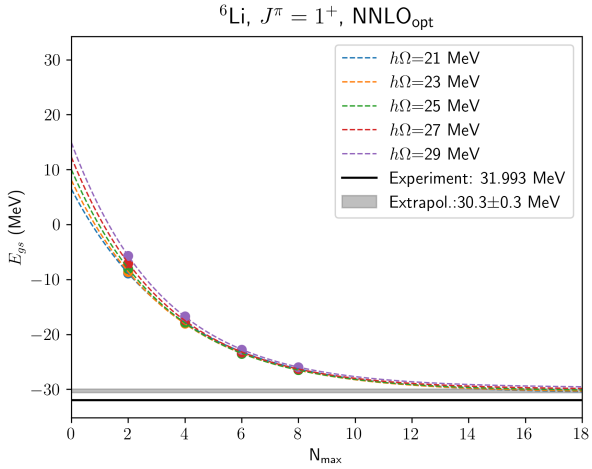

Figure 1.5: Fits of the binding energies of the ground state of ^{6}Li, $J^\pi = 1^+$ at different values of $\hbar\Omega$ and the extrapolated value, calculated with the NNLO$_{\text{opt}}$ potential

identify $\hbar\Omega$ of the minimum for the highest $\mathrm{N_{max}}$ used. One then selects energies at one value of $\hbar\Omega$ below and at three higher, which gives us five data points, including the minimum. Next, for each of the energies selected in the previous step, we fit an exponential plus constant to that energy and to three energy values at the same $\hbar\Omega$ but at lower values of $\mathrm{N_{max}}$. In other words, to the four successive energy values at constant $\hbar\Omega$ we fit the exponential

$$E_{gs}(\mathrm{N_{max}}) = a\exp(-b\mathrm{N_{max}}) + E_{gs}(\infty), \tag{1.3.1}$$

where a, b are free constants and $E_{gs}(\infty)$ represents the converged value of energy. The successive data points are weighed according to

$$\sigma_{\mathrm{N_{max}}} = E_{gs}(\mathrm{N_{max}}) - E_{gs}(\mathrm{N_{max}} - 2) \tag{1.3.2}$$

and the weight for the data point corresponding to the lowest $\mathrm{N_{max}}$ is estimated as three times the weight of the second point. The fitted exponentials for constant

$\hbar\Omega$ values should have the same asymptote because E_{gs} at $N_{max} \to \infty$ should be independent of $\hbar\Omega$. In practice, however, the asymptotes for different $\hbar\Omega$ are spread around a certain value. We take half of this spread as the extrapolation error. Figure 1.5 shows the exponential dependence of the binding energy of ^{6}Li ground state on N_{max}.

The extrapolation method described above is known as the 'global extrapolation method' [15] (or 'Extrapolation A'), since by choosing the 5 $\hbar\Omega$ values we cover a large range of the calculated data. Another way to find the extrapolated energy is to fit (1.3.1) to only the three highest N_{max} values at a constant $\hbar\Omega$. This extrapolation is referred to as 'Extrapolation B'. We usually choose the $\hbar\Omega$ at which the extrapolation is the most stable - the difference between extrapolated value and the calculated minimum is the lowest.

The procedure described above may seem rather arbitrary, but it was shown that it reproduces experimental values quite well [15]. Other procedures that are motivated by EFT exist [16], but the fitted functions have 5 parameters and therefore require calculations for at least 5 different values N_{max}.

1.4 The Symmetry-Adapted NCSM

So far, we have studied the atomic nucleus as a problem of many interacting particles while largely ignoring the collective degrees of freedom. In the following sections, we first take a step back to explain some relevant concepts from group theory on the example of the SO(3) group. We then expand upon it by introducing the Elliott model, which explains nuclear deformations and rotations in terms of the SU(3) group. Our goal in this chapter is then the introduction of the framework of SA-NCSM which utilizes the SU(3) symmetry of nuclei and bridges the gap between collective descriptions of nuclei and the NCSM.

1.4.1 The SO(3) Group

The SO(3) group is a group of all proper orthogonal rotations (i.e., we exclude reflections) in three-dimensional space. The operator that rotates a vector by an angle ϕ can be expressed as

$$U = \exp\left(-\frac{i}{\hbar}\phi \boldsymbol{n}\cdot\boldsymbol{L}\right), \tag{1.4.1}$$

where $\boldsymbol{n}$ is a unit vector in the direction of the axis of rotation and $\boldsymbol{L} = (L_x, L_y, L_z)$ is the angular momentum operator. The operators $\boldsymbol{L}$ are therefore generators of rotations and hence they are generators of the group SO(3). Equivalently, the operators $L_{1\pm1} = L_x \pm iL_y$ together with operator L_z form another set of generators. The generators satisfy the commutation relations

$$\begin{aligned} [L_x, L_y] &= iL_z, \\ [L_z, L_x] &= iL_y, \\ [L_y, L_z] &= iL_x \end{aligned} \tag{1.4.2}$$

and they therefore form a Lie algebra.

The natural basis for the generators od SO(3) group $\boldsymbol{L}$ is labelled as $|lm\rangle$. A representation of a group can be constructed in the basis of its generators. In the case of $l = 1$ the representation would be given by three three-dimensional matrixes comprised of matrix elements $\langle 1m|L_x|1m'\rangle$, $\langle 1m|L_y|1m'\rangle$ and $\langle 1m|L_z|1m'\rangle$. Here, we have constructed a group representation for a fixed value of l. In general, matrix elements $\langle lm|L_i|l'm'\rangle$ do not connect states with different values of l. Such representation is called an *irreducible representation* or an *irrep*. In the case of SO(3), a single irrep has a dimension of $2l + 1$.

It can be easily shown that the quadratic operator $\boldsymbol{L}^2$ commutes with every generator of the SO(3) group. Such an operator is called a *Casimir operator*. The eigenvalue $l(l + 1)$ of the Casimir operator $\boldsymbol{L}^2$ completely labels a single representation of the SO(3) group. The quantum number m of the generator L_z then labels the basis states within that representation, which are representations of the SO(2) group. We have thus constructed the group reduction chain

$$\begin{array}{ccccc} \mathrm{SO}(3) & \supset & \mathrm{SO}(2), \\ l & & m \end{array} \tag{1.4.3}$$

where the SO(2) group describes rotations in a plane and is isomorphic to the group U(1), the group of the unit circle.

1.4.2 The SU(3) Group

The SU(3) group is a group that describes the symmetry of a three-dimensional harmonic oscillator [17]. The generators of this group can be written in the form of spherical tensors as

$$L_{10} = -i(C_{12} - C_{21}), \tag{1.4.4}$$

$$L_{1\pm1} = \frac{1}{\sqrt{2}}((C_{13} - C_{31}) \pm i(C_{23} - C_{32})), \tag{1.4.5}$$

$$Q^a_{20} = 2C_{33} - C_{11} - C_{22} \tag{1.4.6}$$

$$Q^a_{2\pm1} = \mp\sqrt{\frac{3}{2}}\left[(C_{13} + C_{31}) \pm i(C_{23} + C_{32})\right] \tag{1.4.7}$$

$$Q^a_{2\pm2} = \sqrt{\frac{3}{2}}\left[(C_{11} + C_{22}) \pm i(C_{21} + C_{12})\right], \tag{1.4.8}$$

where we define

$$C_{kl} = \frac{1}{2}\sum_{i=1}^{A} b^\dagger_{ik} b_{il} + b_{il} b^\dagger_{ik}, \tag{1.4.9}$$

where $k, l = 1, 2, 3 = x, y, z$ and $b^{(\dagger)}_{ik}$ are the harmonic oscillator ladder operators of the i-th particle, which have the coordinate representation

$$b_{ik} = \sqrt{\frac{m\Omega}{2\hbar}}\left(r_{ik} - \frac{i}{m\Omega}p_{ik}\right), \tag{1.4.10}$$

$$b^\dagger_{ik} = \sqrt{\frac{m\Omega}{2\hbar}}\left(r_{ik} + \frac{i}{m\Omega}p_{ik}\right). \tag{1.4.11}$$

Three of the SU(3) generators are the standard angular momentum operators and the SO(3) is therefore a subgroup of SU(3). The remaining 5 generators are known as algebraic quadrupole moments and we will speak of them in more detail in the following section. The quadratic SU(3) Casimir operator can be written as [18]

$$C_{\mathrm{SU(3)}} = \frac{4}{3}\boldsymbol{Q}^a\cdot\boldsymbol{Q}^a + \frac{1}{2}\boldsymbol{L}\cdot\boldsymbol{L}. \tag{1.4.12}$$

This operator indeed commutes with all the above-listed generators, which can be verified by expressing it in terms of the operators C_{kl} and using the commutation relations

$$\begin{aligned} [b_{ik}, b^\dagger_{jl}] &= \delta_{ij}\delta_{kl}, \\ [b_{ik}, b_{jl}] &= 0, \\ [b^\dagger_{ik}, b^\dagger_{jl}] &= 0. \end{aligned} \tag{1.4.13}$$

In section 1.4.1, we have been able to construct a natural basis by identifying irreps of the SO(3) group. The same can be done for the SU(3) group, but in this case, two labels are needed, usually denoted as λ and μ [17, 19]. We can construct a chain of group reductions

$$\begin{array}{ccccccc} \mathrm{SU(3)} & \supset & \mathrm{SO(3)} & & & & \\ & & \otimes & & \supset \mathrm{SU_J(2)} & \supset & \mathrm{U(1)} \\ & & \mathrm{SU_S(2)} & & & & \\ (\lambda\mu) & \kappa & (LS) & & J & & M_J \end{array}$$

where we have coupled the quantum numbers of total angular momentum L and total spin S into J by considering the product $\mathrm{SU(3)}\otimes\mathrm{SU_S(2)}$. We are already familiar with the SU(3) and SO(3) groups of this chain but have not yet mentioned the SU(2) group. This group can be used to describe the rotations of spinors and total angular momentum vectors. There exists a homomorphism between the SU(2) and SO(3) groups, each two elements of SU(2) correspond to one element of SO(3) [3]. A single $\mathrm{SU(3)}\otimes\mathrm{SU_S(2)}$ state $|\psi\rangle$ is then labeled as

$$|\psi\rangle = |(\lambda\mu)\kappa(LS)JM_J\rangle, \tag{1.4.14}$$

where the number κ describes the multiplicity of L within a single SU(3) irrep. To deal with the fact that the nucleus contain two types of fermions, protons and neutrons, we can indroduce another degree of freedom into the state 1.4.14, isospin T and its projection M_T. Just like spin, isospin is described by the SU(2) group. A single $\mathrm{SU(3)}\otimes\mathrm{SU_S(2)}\otimes\mathrm{SU_T(2)}$ state $|\psi\rangle$ is therefore described by the quantum numbers

$$|\psi\rangle = |(\lambda\mu)\kappa(LS)JM_J; TM_T\rangle. \tag{1.4.15}$$

Alternatively, one can construct antisymmetric SU(3) irreps separately for protons and neutrons and then couple them into a total wavefunction

$$|\psi\rangle = |(\lambda_\pi\,\mu_\pi)S_\pi \times (\lambda_\nu\,\mu_\nu)S_\nu; (\lambda\mu)\kappa(LS)JM_J\rangle, \tag{1.4.16}$$

which is antisymmetric only under the exchange of protons and neutrons. The above introduced labeling scheme is known as *the SU(3) scheme*.

1.4.3 Elliott SU(3) Model

The Elliott model assumes that the shell model residual interaction introduced in (1.1.2) has a quadrupole character and the Hamiltonian can be written as [18]

$$H = H_0 - \chi \boldsymbol{Q}^a \cdot \boldsymbol{Q}^a, \tag{1.4.17}$$

where H_0 is the harmonic oscillator Hamiltonian

$$H_0 = \sum_{i=1}^{A} \frac{p_i^2}{2m_n} + \frac{1}{2} m_n \omega^2 r_i^2 \tag{1.4.18}$$

and χ describes the coupling strength. The quadrupole interaction is given by the product $\boldsymbol{Q}^a \cdot \boldsymbol{Q}^a = \sum_q (Q^a_{2q})^\dagger Q^a_{2q}$ of algebraic quadrupole operators Q^a_{2q} that are defined in coordinate representation as

$$Q^a_{2q} = \sqrt{\frac{4\pi}{5}} \frac{1}{b^2} \sum_{i=1}^{A} \left[\boldsymbol{r}_i^2 Y_{2q}(\hat{\boldsymbol{r}}_i) + b^4 \boldsymbol{p}_i^2 Y_{2q}(\hat{\boldsymbol{p}}_i) \right], \tag{1.4.19}$$

where the index q is equal to $0, \pm 1, \pm 2$ and Y are the usual spherical harmonics that depend on a unit vector in the direction of momentum or position of the i-th particle, $\hat{\boldsymbol{p}}_i$ or $\hat{\boldsymbol{r}}_i$. It is important to note that this operator differs from the mass quadrupole operator

$$Q^c_{2q} = \sqrt{\frac{16\pi}{5}} \frac{1}{b^2} \sum_{i=1}^{A} \left[\boldsymbol{r}_i^2 Y_{2q}(\hat{\boldsymbol{r}}_i) \right] \tag{1.4.20}$$

by the inclusion of the momentum dependant term. The matrix elements of the algebraic operator Q^a_{2q} equals to zero for different major oscillator shells $n \neq n'$. This can be easily proved by considering the equations (1.4.6), (1.4.7) and (1.4.8).

The harmonic oscillator Hamiltonian (1.4.18) can be rewritten in terms of C_{kl} as

$$H_0 = C_{11} + C_{22} + C_{33} \tag{1.4.21}$$

and it can be easily verified by using the commutation relations (1.4.13) that for every k, l

$$[H_0, C_{kl}] = 0. \tag{1.4.22}$$

This means that the HO Hamiltonian commutes with each and every generator of SU(3) and we can label its eigenstates with the SU(3) irrep labels, i.e., the SU(3) scheme. The labels λ and μ can then be interpreted [17, 19] as

$$\lambda = N_z - N_x, \tag{1.4.23}$$

$$\mu = N_x - N_y, \tag{1.4.24}$$

where N_i is the total number of oscillator quanta in the i-th cartesian direction.

The quadrupole interaction of the Elliott Hamiltonian can be expressed using the quadratic Casimir operator of the SU(3) group as

$$\boldsymbol{Q}^a \cdot \boldsymbol{Q}^a = \frac{3}{4} C_{\mathrm{SU(3)}} - \frac{3}{8} \boldsymbol{L} \cdot \boldsymbol{L} \tag{1.4.25}$$

and the expectation value of $C_{\mathrm{SU}(3)}$ is given by [18]

$$\langle \lambda\mu | C_{\mathrm{SU}(3)} | \lambda\mu \rangle = \frac{2}{3}(\lambda^2 + \lambda\mu + \mu^2 + 3\lambda + 3\mu). \tag{1.4.26}$$

For the energies $E_{(\lambda\mu)L} = \langle (\lambda\mu)L|H|(\lambda\mu)L\rangle$ of the Elliott Hamiltonian we then obtain

$$E_{(\lambda\mu)L} = N_0\hbar\Omega - \frac{1}{2}\chi(\lambda^2 + \lambda\mu + \mu^2 + 3(\lambda+\mu)) + \frac{3}{8}\chi L(L+1), \tag{1.4.27}$$

where $N_0\hbar\Omega$ are energies of the HO Hamiltonian. We see that energies within a single SU(3) irrep are proportional to $L(L+1)$. Also, the states with the lowest energies are states with the maximal value of $\langle C_{\mathrm{SU}(3)}\rangle$.

The SU(3) states of the Elliott model can be interpreted geometrically in terms of the quadrupole nuclear shape variables β, γ, which were introduced by A. Bohr and B.R. Mottelson [20]. The parameter β describes the scale of the deformation and γ the degree of nonaxiality. Their meaning is illustrated in the figure 1.6. The relationship of the shape variables and SU(3) labels can be derived

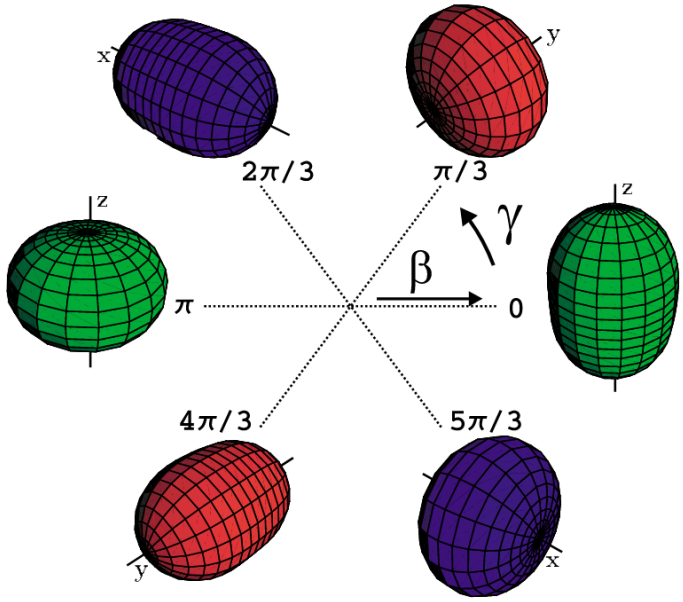

Figure 1.6: The nuclear shape variables and related shapes. The parameter β can be thought of as a radius and γ as the angle of a polar plot. Figure adapted from [21].

from the relationships of Lie algebras of the Elliott model and the quantum rigid rotor [22]. The formulae one obtains are

$$k\beta\cos\gamma = \frac{2\lambda + \mu + 3}{3}, \tag{1.4.28}$$

$$k\beta\sin\gamma = \frac{\mu + 1}{\sqrt{3}}, \tag{1.4.29}$$

where $k^2 = (5/9\pi)(A\langle r^2\rangle)$ and $\langle r^2\rangle$ is the nuclear mean square radius. The equations (1.4.28) and (1.4.29) define a map $(\lambda, \mu) \to (\beta, \gamma)$. It is important to

note that since λ and μ are representation labels, they must be non-negative and can be equal to only certain discrete values. This points to a discrepancy between microscopic and collective nuclear models and places constraints on the shapes a nucleus is allowed to have.

From (1.4.28) and (1.4.29) we can also deduce the fact that irreps with $\mu = 0$ correspond to prolate shapes and irreps with $\lambda = 0$ to oblate shapes. Irreps, where both labels are zero, describe a spherical nucleus (Fig 1.7).

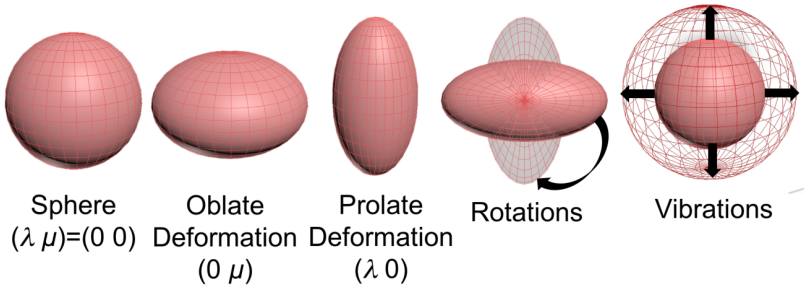

Figure 1.7: Various collective modes of nuclei and their relationship to the SU(3) quantum labels λ and μ. Figure adapted from [23].

1.4.4 The Basis of the SA-NCSM

As we have found out earlier, the wavefunctions of the Elliott model can be constructed only in a single major oscillator shell. The SA-NCSM generalizes the Elliott model and utilizes the SU(3) scheme in the ab initio framework of the NCSM. Each of the many-particle basis states is labeled as

$$|\gamma N(\lambda\mu)\kappa L; (S_p S_n)S; JM\rangle, \tag{1.4.30}$$

where N is total number of HO excitation quanta, S_p (S_n) is the spin of protons (neutrons) and S is the total spin. The symbol γ represents any additional quantum numbers, which are needed to distinguish between configurations with the same $N(\lambda\,\mu)$ and $(S_p\,S_n)S$. The center of mass motion can be factored using the same technique, which we have discussed for the NCSM [8].

The use of the SU(3) basis is very advantageous since it allows to study collective properties of nuclei in the framework of a microscopic model. We can select a model space that contains only a few physically relevant states, and therefore we are able to reach higher values of $\mathrm{N_{max}}$ than in the standard NCSM and obtain better-converged results. Furthermore, the dominant states in $N\hbar\Omega$ shells seem to follow a pattern given by

$$N + \lambda_0 + 2\mu_0 = \lambda + 2\mu, \tag{1.4.31}$$

where $(\lambda_0\,\mu_0)$ label the dominant state of the $0\hbar\Omega$ shell [24]. In practice, we select a full space for certain $N^{\perp}_{\mathrm{max}}$, where our choice depends on the mass of the studied nucleus and available computing power, and then with the help of the above formula, we try to select a few physically relevant states from spaces higher than $N^{\perp}_{\mathrm{max}}$ up until $N^{\top}_{\mathrm{max}}$. We can therefore characterize our model space by two numbers $\langle N^{\perp}_{\mathrm{max}}\rangle N^{\top}_{\mathrm{max}}$. This kind of model space truncation will be discussed more in the third chapter, where we will present our results for concrete nuclei.

2. Beta Decay

2.1 General Description

Nuclear β^- decay is a process mediated by the weak interaction, in which the initial nucleus is transformed into a nucleus with the same mass number A while the number of protons Z is increased by one

$$ {}^{\mathrm{A}}_{\mathrm{Z}}\mathrm{X} \rightarrow {}^{\mathrm{A}}_{\mathrm{Z+1}}\mathrm{Y} + e^- + \bar{\nu}_e, \tag{2.1.1} $$

and an electron e^- with an electron anti-neutrino $\bar{\nu}_e$ are emitted. In the β^+ decay

$$ {}^{\mathrm{A}}_{\mathrm{Z}}\mathrm{X} \rightarrow {}^{\mathrm{A}}_{\mathrm{Z-1}}\mathrm{Y} + e^+ + \nu_e, \tag{2.1.2} $$

the proton number is decreased by one while a positron e^+ and an electron neutrino ν_e are emitted. Beta decay can thus be thought of as the decay of a neutron or a proton in the nuclear medium. Note that the decay of a free neutron is possible, but the decay of a free proton is not allowed due to the conservation of mass.

2.1.1 Fermi and Gammow-Teller Operators

Beta decay is induced by the Fermi and Gammow-Teller operators, which are the simplest operators that can be constructed so the selection rules of β decay transitions are reproduced. They are defined as

$$ F^{\pm} = \sum_{k=1}^{A} \tau_{\pm,k} \tag{2.1.3} $$

and

$$ (\mathrm{GT})^{(\pm)} = \sum_{k=1}^{A} \boldsymbol{\sigma}_k \tau_{\pm,k}, \tag{2.1.4} $$

respectively [4, 5].

The operator τ_- is the isospin lowering operator and is responsible for the transformation of a neutron into a proton, while τ_+ is the isospin raising operator and is responsible for the opposite transformation $p \rightarrow n$. The $\boldsymbol{\sigma}_k$ in 2.1.3 is the Pauli spin operator. It follows that the Fermi operator cannot change the total isospin of the nucleus but causes it to transition to a nucleus with a different total isospin projection M_T (the proton number Z is changed, while A remains the same). The Gamow-Teller operator changes not only the isospin projection but can also change the spin projection of the nucleus. Since $\boldsymbol{\sigma}$ is a vector operator (i.e., spherical tensor of rank $J_0 = 1$), it has three spherical components $0, \pm 1$ that correspond to a change of total spin $\Delta S = 0, \pm 1$, respectively. Note that since the Fermi operator consists only of the isospin lowering/raising operator, the summation can be done explicitly and we get the total isospin lowering/raising operator

$$ \sum_{k=1}^{A} \tau_{\pm,k} = T^{\pm}, \tag{2.1.5} $$

which raises or lowers the isospin projection of the whole nucleus.

2.1.2 Classifaction of β-decays

Each of the leptons in decays 2.1.1 and 2.1.2 has spin $s = 1/2$. The difference between the initial and the final total angular momentum of the nuclear state can be either $\Delta J = 0$ or $\Delta J = 1$, assuming the emitted leptons are in an s state with $l = 0$ and therefore do not carry any angular momentum but spin. Transitions of this type are called allowed. For $\Delta J = 0$, the transition can be induced by both Fermi and GT operators. On the other hand, $\Delta J = 1$ transitions can be induced only by the GT operator. The selection rules of Fermi and Gamow-Teller transitions are summarized in table 2.1.

Table 2.1: Allowed β-decay selection rules

Transition	ΔJ	$\pi_i \pi_f$
Fermi	0	+1
GT	1 ($J_i = 0$ or $J_f = 0$)	+1
GT	0,1 ($J_i > 0$ and $J_f > 0$)	+1

The half-life of a nucleus is given by the equation

$$t_{1/2} = \frac{\ln 2}{T_{fi}}, \tag{2.1.6}$$

where T_{fi} is the decay transition probability. Using Fermi's golden rule [4], one can obtain the following expression

$$t_{1/2} = \frac{K}{f_0(B_F + B_{GT})}, \tag{2.1.7}$$

where f_0 is the phase-space integral that describes lepton kinematics and the constant K is given by

$$K = \frac{2\pi^3 \hbar^7}{m_e^5 c^4 G_F^2}, \tag{2.1.8}$$

where G_F is the fundamental coupling constant of the weak interaction. The reduced Fermi and Gamow-Teller transition probabilities B_F and B_{GT} are equal to

$$B_F = \frac{g_V}{2J_i + 1} |M_F|^2, \quad B_{GT} = \frac{g_A}{2J_i + 1} |M_{GT}|^2, \tag{2.1.9}$$

where g_V and g_A are constants related to the fundamental coupling constant of the weak interaction, as will be discussed later in section 2.2.3 and M_F (M_{GT}) are the reduced matrix elements of the Fermi (Gamow-Teller) operator.

Experimental values of beta transitions are usually given in the so-called 'log ft' values defined as

$$\log ft = \log_{10}(f_0 t_{1/2}), \tag{2.1.10}$$

f_0 is dimensionless and the half-life is expressed in seconds.

The table 2.2 shows the classification of β-decays according to different values of $\log ft$. The superallowed β-decays conform to the selection rules discussed above and occur in light nuclei, where the wavefunction of the nucleus before and after decay is left almost unchanged. The Fermi and GT transition probabilities

are highest for this type of decay. Superallowed decays are especially important as they can be used to look for physics beyond the standard model, as will be discussed in section 2.2.

The l-forbidden transitions break the $\Delta l = 0$ selection rule but conform to the other rules. Unfavoured allowed transitions belong to neither of the mentioned groups. The selection rules are upheld, but the transition is hindered by the nuclear structure effects.

Table 2.2: Classifaction of β-decays [4].

Transition	$\log ft$
superallowed	2.9-3.7
unfavoured allowed	3.8-6.0
l-forbidden allowed	$\geq$5.0

2.1.3 Decay Matrix Elements in Terms of SU(2) Tensors

To calculate probabilities of Fermi and Gamow-Teller transitions, we need to first derive the formulae for the reduced matrix elements of the respective operators. We will use the formula

$$\langle J_f||T^{J_0}||J_i\rangle = \frac{1}{\sqrt{2J_0+1}}\sum_{ab}\langle a||T^{J_0}||b\rangle\langle J_f||[a_a^\dagger \times \tilde{a}_b]^{J_0}||J_i\rangle, \tag{2.1.11}$$

which holds true for any spherical (SU(2)) one-body tensor operator of rank J_0 [4]. Here, $|J_i\rangle$ ($|J_f\rangle$) is the initial (final) wavefunction and $a^\dagger$ ($\tilde{a}$) is the particle creation (annihilation) spherical tensor operator. The matrix element $\langle J_f||[a_a^\dagger \times \tilde{a}_b]^{J_0}||J_i\rangle$ is usually referred to as the reduced one-body transition density. The index a (b) is a shorthand for $n_a l_a j_a t_a$ ($n_b l_b j_b t_b$). Applying this expression to (2.1.3) we get

$$\begin{aligned}\langle J_f||\sum_{i=1}^{A}\tau_{\pm,a}||J_i\rangle = \delta_{J_i,J_f}\sum_{ab}\sqrt{t_b(t_b+1)-m_{t,b}(m_{t,b}\pm 1)}\ \times \\ \times\ \langle n_a l_a j_a||1||n_b l_b j_b\rangle\langle J_f||[a^\dagger_{n_a l_a j_a}\times\tilde{a}_{n_b l_b j_b}]^{J_0=0}||J_i\rangle,\end{aligned} \tag{2.1.12}$$

where 1 is the unit operator, t and m_t are the isospin and its third component, and the indexes a, b are the proton, neutron index when β^- decay is considered or the opposite for β^+ decay. The square root at the end of the first of line comes from the matrix element $\langle t_a m_{t,a}|\tau^\pm|t_a m_{t,a}\rangle$ and is always equal to one since for nucleons $t = \frac{1}{2}$ and $m_t = \frac{1}{2}$ ($m_t = -\frac{1}{2}$) for neutrons (protons). The reduced matrix elements of the unit operator are simply

$$\langle n_a l_a j_a||1||n_b l_b j_b\rangle = \delta_{n_a,n_b}\delta_{l_a,l_b}\delta_{j_a,j_b}\sqrt{2j_a+1}. \tag{2.1.13}$$

To calculate GT matrix elements, we shall use the formula (96) provided in [25]

$$\begin{aligned}\langle l_f s_f j_f||\boldsymbol{\sigma}||l_i s_i j_i\rangle = (-1)^{l_i+s_i+j_f+1}\delta_{l_i,l_f}\delta_{s_i,s_f}\ \times \\ \times\ 2\sqrt{s_i(s_i+1)(2s_i+1)(2j_f+1)(2j_i+1)}\begin{Bmatrix} s_i & l & j_i \\ j_f & 1 & s_i\end{Bmatrix}.\end{aligned} \tag{2.1.14}$$

In our case $s_f = s_i = \frac{1}{2}$, $j_f = j_a$ and $j_i = j_b$. Plugging in these values and using the fact that the Wigner 6j symbol is invariant under the interchange of the upper and lower arguments in any of the two columns [25], we get

$$\langle n_a l_a j_a || \boldsymbol{\sigma} || n_b l_b j_b \rangle = \sqrt{6}(-1)^{l_a + j_a + \frac{3}{2}} \delta_{n_a,n_b} \delta_{l_a,l_b} \times \\ \times \sqrt{(2j_a+1)(2j_b+1)} \begin{Bmatrix} \frac{1}{2} & \frac{1}{2} & 1 \\ j_a & j_b & l_a \end{Bmatrix}. \quad (2.1.15)$$

We have obtained the following expressions for the reduced matrix elements M_F of the Fermi operator and for the reduced matrix elements M_{GT} of the Gammow-Teller operator

$$M_F \equiv \delta_{J_i,J_f} \sum_{ab} \delta_{n_a,n_b} \delta_{l_a,l_b} \delta_{j_a,j_b} \sqrt{2j_a+1} \langle J_f || [a^\dagger_{n_a l_a j_a} \times \tilde{a}_{n_b l_b j_b}]^{J_0=0} || J_i \rangle, \quad (2.1.16)$$

$$M_{GT} \equiv \sqrt{2} \sum_{ab} (-1)^{l_a + j_a + \frac{3}{2}} \delta_{n_a,n_b} \delta_{l_a,l_b} \sqrt{(2j_a+1)(2j_b+1)} \times \\ \times \begin{Bmatrix} \frac{1}{2} & \frac{1}{2} & 1 \\ j_a & j_b & l_a \end{Bmatrix} \langle J_f || [a^\dagger_{n_a l_a j_a} \times \tilde{a}_{n_b l_b j_b}]^{J_0=1} || J_i \rangle. \quad (2.1.17)$$

2.1.4 Decay Matrix Elements in Terms of SU(3) Tensors

In the previous section, we have derived the Fermi and Gammow-Teller reduced matrix elements in terms of spherical tensors. However, for them to be compatible with the SA-NCSM, we need to find their representation in terms of SU(3) tensors. The reduced transition density matrix element of 2.1.11 can be transformed into the SU(3) tensor representation using the relation [26]

$$\langle J_f || [a^\dagger_{n_a l_a j_a} \times \tilde{a}_{n_b l_b j_b}] || J_i \rangle = (-)^{n_b} \sum_{(\lambda_0,\mu_0) S_0 \kappa_0 L_0} \Pi_{j_a j_b L_0 S_0} \times \\ \times \langle (n_a\, 0) l_a; (0\, n_b) l_b || (\lambda_0\, \mu_0) \kappa_0\, L_0 \rangle \begin{Bmatrix} l_a & l_b & L_0 \\ 1/2 & 1/2 & S_0 \\ j_a & j_b & J_0 \end{Bmatrix} \times \quad (2.1.18) \\ \times \langle J_f || \left[a^{\dagger (n_a\, 0)} \times \tilde{a}^{(0\, n_b)} \right]^{(\lambda_0\, \mu_0) S_0}_{\kappa_0\, L_0\, J_0} || J_i \rangle,$$

where $\langle ; || \rangle$ is the reduced SU(3) Clebsch-Gordan coefficient that couples different $(\lambda\, \mu)$ irreps and Π_k is the notation for $\sqrt{2k+1}$. The operators $a^\dagger_{n_a l_a j_a}$ and $\tilde{a}_{n_b l_b j_b}$ are the creation and annihilation spherical tensors, the operators $a^{\dagger (n_a\, 0)}$ and $\tilde{a}^{(0\, n_b)}$ are the particle creation and annihilation SU(3) tensors, which create a particle with spin one-half in the n_a shell and annihilate a particle with spin one-half in the n_b shell.

To obtain the reduced matrix element M_F in terms of SU(3) tensors, we need to substitute (2.1.4) into (2.1.16). Since the Fermi operator (2.1.3) does not act on any of the SU(3)$\otimes$SU$_\mathrm{S}$(2) quantum numbers the sum in (2.1.4) reduces to a single term with $(\lambda_0\, \mu_0) = (0\, 0)$, $S_0 = 0$, $L_0 = 0$ and $\kappa_0 = 0$. The Wigner 9j symbol then simplifies into the form

$$\begin{Bmatrix} l_a & l_b & 0 \\ 1/2 & 1/2 & 0 \\ j_a & j_b & 0 \end{Bmatrix} = \frac{\delta_{j_a j_b} \delta_{l_a l_b}}{\sqrt{2(2l_a+1)(2j_a+1)}} \quad (2.1.19)$$

and for the reduced SU(3) Clebsch-Gordan coefficients we obtain [27]

$$\langle (n\,0)l;(0\,n)l||(0\,0)0\,0\rangle = \sqrt{2}(-)^n\sqrt{\frac{2l+1}{(n+1)(n+2)}}. \tag{2.1.20}$$

Substituting into (2.1.16), we get

$$M_F = (-)^n\sum_{nlj}\frac{2j+1}{\sqrt{(n+1)(n+2)}}\langle J_f||[a^{\dagger(n\,0)}\times\tilde{a}^{(0\,n)}]^{(\lambda_0=0\,\mu_0=0)S_0=0}_{\kappa_0=0\;L_0=0\;J_0=0}||J_i\rangle. \tag{2.1.21}$$

The last equation can be further simplified. Since only the numerator $2j+1$ depends explicitly on j, l we can single out the sum $\sum_{lj} 2j+1$, which is equal to

$$\sum_{lj} 2j+1 = \sum_{l}^{n}(2l-1+1)+(2l+1+1) = \sum_{l}^{n} 4l+2, \tag{2.1.22}$$

where we used the fact that $j = l \pm 1/2$ for nucleons. The sum goes over all possible values of l, which are odd or even since $l = n, n-2, n-4, ..., 1\,\text{or}\,0$. For both even or odd values of l, the sum is equal to

$$\sum_{l}^{n} 4l+2 = (n+1)(n+2). \tag{2.1.23}$$

The reduced matrix element of the Fermi operator represented in the SU(3) tensorial form then becomes

$$M_F = \sum_{n}\sqrt{(n+1)(n+2)}\,\langle J_f||[a^{\dagger(n\,0)}\times\tilde{a}^{(0\,n)}]^{(\lambda_0=0\,\mu_0=0)S_0=0}_{\kappa_0=0\,L_0=0\,J_0=0}||J_i\rangle. \tag{2.1.24}$$

We now turn our attention to the GT transition matrix elements. Analogously to Fermi transitions, the λ_0, μ_0, L_0 and κ_0 quantum numbers are equal to 0, but S_0 and J_0 are equal to 1. We can thus write the 9j symbol in (2.1.4) as [25]

$$\begin{Bmatrix} l_a & l_b & 0 \\ 1/2 & 1/2 & 1 \\ j_a & j_b & 1 \end{Bmatrix} = \frac{(-1)^{3/2+j_a+l}}{\sqrt{3(2l+1)}}\begin{Bmatrix} 1/2 & 1/2 & 1 \\ j_a & j_b & l \end{Bmatrix}, \tag{2.1.25}$$

where we have used the fact that angular momentum in a GT transition is conserved and thus $l_a = l_b$. Using (2.1.20) and (2.1.17) we can then write

$$M_{GT} = \sum_{nlj_aj_b}(-)^n\frac{2(2j_a+1)(2j_b+1)}{\sqrt{(n+1)(n+2)}}\begin{Bmatrix} 1/2 & 1/2 & 1 \\ j_b & j_a & l \end{Bmatrix}\begin{Bmatrix} 1/2 & 1/2 & 1 \\ j_b & j_a & l \end{Bmatrix}\times$$
$$\times\langle J_f||[a^{\dagger(n\,0)}\times\tilde{a}^{\dagger(0\,n)}]^{(\lambda_0\,\mu_0)S_0}_{\kappa_0\;L_0\;J_0}||J_i\rangle \tag{2.1.26}$$

This formula can be further simplified. We first single out the part that does not depend explicitly on n

$$\sum_{lj_aj_b}^{n}(2j_a+1)(2j_b+1)\begin{Bmatrix} 1/2 & 1/2 & 1 \\ j_b & j_a & l \end{Bmatrix}\begin{Bmatrix} 1/2 & 1/2 & 1 \\ j_b & j_a & l \end{Bmatrix}, \tag{2.1.27}$$

where $j_a = l \pm 1/2$, $j_b = l \pm 1/2$ and we have to account for all possibilities since for a GT transition $\Delta J = 0, 1$. Writing out the sum explicitly, we get

$$\begin{aligned}
&\sum_{l}^{n}(2l+2)^2 \begin{Bmatrix} 1/2 & 1/2 & 1 \\ l+1/2 & l+1/2 & l \end{Bmatrix} \begin{Bmatrix} 1/2 & 1/2 & 1 \\ l+1/2 & l+1/2 & l \end{Bmatrix} + \\
&+ 4l(2l+2) \begin{Bmatrix} 1/2 & 1/2 & 1 \\ l-1/2 & l+1/2 & l \end{Bmatrix} \begin{Bmatrix} 1/2 & 1/2 & 1 \\ l-1/2 & l+1/2 & l \end{Bmatrix} + \\
&+ 4l^2 \begin{Bmatrix} 1/2 & 1/2 & 1 \\ l-1/2 & l-1/2 & l \end{Bmatrix} \begin{Bmatrix} 1/2 & 1/2 & 1 \\ l-1/2 & l-1/2 & l \end{Bmatrix},
\end{aligned} \tag{2.1.28}$$

where we have made use of the symmetries of 6j symbols in the middle row. Using the algebraic expression for 6j symbols from the table 9.1. in [25], we obtain

$$\begin{Bmatrix} 1/2 & 1/2 & 1 \\ l+1/2 & l+1/2 & l \end{Bmatrix} = \frac{1}{2}\left[\frac{2(2l+3)}{3(2l+1)(2l+2)}\right]^{\frac{1}{2}}, \tag{2.1.29}$$

$$\begin{Bmatrix} 1/2 & 1/2 & 1 \\ l-1/2 & l+1/2 & l \end{Bmatrix} = (-)^{2l+1}\frac{1}{\sqrt{3}\sqrt{2l+1}}, \tag{2.1.30}$$

$$\begin{Bmatrix} 1/2 & 1/2 & 1 \\ l-1/2 & l-1/2 & l \end{Bmatrix} = \frac{1}{2}\left[\frac{2(2l-1)}{3(2l)(2l+1)}\right]^{\frac{1}{2}}. \tag{2.1.31}$$

Now we can simplify the sum (2.1.27). By plugging (2.1.29) into (2.1.28) we get

$$\sum_{l}^{n}\frac{1}{6(2l+1)}\left((2l+2)(2l+3)+8l(2l+2)+2l(2l-1)\right) = \tag{2.1.32}$$

$$= \sum_{l}^{n}\frac{1}{6(2l+1)}\left(6(2l+1)^2\right) = \sum_{l}^{n} 2l+1 = \frac{1}{2}(n+1)(n+2), \tag{2.1.33}$$

where we have recognized that the final sum is just half of the sum we have already calculated earlier. Hence, for the GT matrix element in the SU(3) tensor representation, we obtain

$$M_{GT} = \sum_{n}\sqrt{(n+1)(n+2)}\langle J_f||[a^{\dagger(n\,0)} \times \tilde{a}^{(0\,n)}]^{(\lambda_0=0\,\mu_0=0)S_0=1}_{\kappa_0=0\,L_0=0\,J_0=1}||J_i\rangle. \tag{2.1.34}$$

Note that the reduced matrix elements (2.1.24) and (2.1.34) have to be multiplied by the factor $\sqrt{2J_f+1}$ when calculated with the SA-NCSM since its implementation `LSU3Shell` [28] uses a convention, where the reduced matrix element in the Wigner-Eckart theorem is not divided by this factor.

2.2 Physics Beyond The Standard Model

The recent progress in ab initio calculation of atomic nuclei has made it possible to calculate matrix elements of various operators and observables with very high accuracy. Due to this fact, ab initio models can be used to test physical theories in conjunction with nuclear and particle physics experiments. In this section, we will outline some examples where nuclear ab initio calculations can be used to look for physics beyond the standard model.

2.2.1 Search for Tensor and Scalar Currents

Up until the 1950's all interactions in nature were thought to be parity-conserving, i.e., invariant to spatial inversion. However, around that time, it was experimentally proven [29] by studying the β decay of ^{60}Co that the weak interaction breaks this symmetry. It was shown that the leptons emitted during β^+ decay are left-handed, which means that their spin and momentum vectors point in exactly opposite directions. On the other hand, the anti-leptons emitted in β^- decay are right-handed. This would then imply that the weak interaction Lagrangian must contain only vector and axial-vector terms with asymmetric contributions since contributions of other types (scalar, pseudoscalar, or tensor) would produce leptons that are not strictly left-handed in β^+ decays and strictly right-handed in β^- decays. This is known as the vector minus axial-vector (V-A) structure of the weak force and the Fermi operator and Gamow-Teller operators representing vector and axial-vector parts of the weak interaction are a direct consequence of this theory [30].

The Fermi and Gamow-Teller operators that were discussed in the previous sections are, in reality, only the zeroth order approximation. When one takes the so-called recoil effects into account, terms proportional to q/m_n, where q is the momentum transfer, must be included in the formulae for M_F and M_{GT}. Their contributions are very small, usually in the order of 1%. Modern experiments can determine the value of β-decay matrix elements with precision as high as 0.1%. Therefore even the small recoil effects are significant [31].

Allowed β-decays such as the decay of ^{8}Li into ^{8}Be [32] provide great testing grounds for these measurements since the impact of the nuclear medium is minimized. Precise calculations of Fermi and Gammow-Teller matrix elements and their recoil corrections in conjunction with modern experiments can offer insight into the V-A theory of electroweak force and validate the existence of tensor or scalar interactions proposed by extensions of the standard model [31].

2.2.2 Neutrinoless Double β-decay

The existence of left-handed and right-handed neutrinos described in the previous section violates both the charge (C) and spatial (P) symmetry separately, but the combined CP symmetry would still be conserved, provided the neutrino is a massless particle. However, currently, it is understood that neutrino has, albeit extremely small, mass. If the neutrino is not massless, then it has a rest frame and the projection of spin onto the direction of momentum, its helicity, can not be used to distinguish between the particle and the anti-particle.

The energy of a massless particle is given by the well-known equation from special relativity

$$|E| = cp \tag{2.2.1}$$

and helicity is given by

$$h = \frac{\boldsymbol{\sigma} \cdot \boldsymbol{p}}{p}. \tag{2.2.2}$$

Combining these two equations, one obtains only four possibilities: the anti-neutrino with $E < 0$ can have positive or negative helicity depending on its spin projection and the same for a neutrino with $E > 0$. For a particle with mass,

different frames of reference exist and the equation (2.2.1) would no longer hold - the helicity would then depend on the frame of reference.

If the neutrino and its anti-particle do not have different intrinsic helicities, they could be the same particle. Particles that are their own anti-particles are known as Majorana particles. In contrast with the standard Dirac particles that are anti-symmetric under CP inversion ($CP = -PC$), Majorana particles are symmetric ($CP = PC$).

One way to resolve the nature of the neutrino is to observe the neutrinoless double-β decay. Such decays could occur when the single decay is energetically impossible, but the double decay into a nucleus with two fewer neutrons is possible. The scheme of this decay would then be

$$ {}^{\mathrm{A}}_{\mathrm{Z}}\mathrm{X} \rightarrow {}_{\mathrm{Z}+2}{}^{\mathrm{A}}\mathrm{Y} + e^- e^- + \bar{\nu}_e \bar{\nu}_e. \tag{2.2.3} $$

In this process, the anti-neutrino from the first decay could act, if we suppose it is of the Majorana type, as the starter for the second decay, during which it would be converted into an electron. We then observe a double β-decay at the end of which no neutrinos can be detected. There are 35 candidates among the nuclei for which the double decay is probable [5].

The matrix elements of such a process can be derived and calculated in the framework of SA-NCSM and insights into the probabilities of neutrinoless double β-decays can be obtained [23].

2.2.3 The Cabibbo–Kobayashi–Maskawa Matrix

The CKM matrix describes the mixing of quark flavors in processes involving the electroweak interaction. The matrix can be expressed in the form [33]

$$ V = \begin{pmatrix} V_{ud} & V_{us} & V_{ub} \\ V_{cd} & V_{cs} & V_{cb} \\ V_{td} & V_{ts} & V_{tb} \end{pmatrix}, \tag{2.2.4} $$

where for example the V_{us} term mixes the up and strange quark states, the V_{ub} term mixes up and bottom quarks and so on. The matrix element V_{ud} is especially important for us since it is directly related to the constant g_V that was introduced in (2.1.9). The conserved vector current (CVC) hypothesis of the standard model predicts that the ft-values of superallowed transitions are related to the fundamental vector coupling constant G_V, the value of which is the same for every transition of this type. The relationship is given by [33]

$$ G_V = G_F g_V V_{ud} = G_F V_{ud}. \tag{2.2.5} $$

where G_F is the Fermi coupling constant and $g_V = 1$ according to CVC. The value of the V_{ud} matrix element is usually determined using superallowed β decay since we want to limit the effects of nuclear structure and the axial-vector current as much as possible.

The CKM matrix is currently thought to be unitary, although experiments have not been conclusive yet. Currently, the most precise values for the matrix elements are [34]

$$ V = \begin{pmatrix} 0.97370(14) & 0.2245(8) & 0.00382(24) \\ 0.221(4) & 0.987(11) & 0.0410(14) \\ 0.0080(3) & 0.0388(11) & 1.013(30) \end{pmatrix}, \tag{2.2.6} $$

The tests of the unitarity of the CKM matrix do not yield any new physics by themselves, but if the unitary were proved, it could put constraints on new physics beyond the standard model.

3. Results

In this chapter, we present results for concrete nuclei. We first discuss the binding energies of light nuclei from $A = 3$ to $A = 16$ calculated with SA-NCSM and their extrapolations. Next, we discuss the low-lying spectrum of ^{16}N, which is a nucleus with very closely spaced ground and excited states and can thus serve as a good benchmark for the accuracy of the ab initio NCSM and the potentials used. The main focus of this chapter is the calculation of the GT operator matrix elements within the SA-NCSM framework for selected nuclei.

3.1 Binding Energies

For the very light nuclei, ^{3}H and ^{3}He binding energies for both potentials are in similar agreement with the experimental value. The dependence of the ground state binding energies on N_{max} and $\hbar\Omega$ for these nuclei are shown on figures 3.1, 3.2 and 3.3, 3.4. The $NNLO_{opt}$ interaction underbinds ^{3}H and ^{3}He by about 240 and 260 keV, respectively. The JISP16 case is similar, although it underbinds ^{3}H by only 100 keV and ^{3}He by about 50 keV. Since the dimension of the basis for $A = 3$ is rather small, we were able to reach N_{max}=12, where the energies are already quite well converged. The variational minima for ^{3}H are -8.161 MeV ($NNLO_{opt}$), -8.340 MeV (JISP16) and for ^{3}He are -7.400 MeV ($NNLO_{opt}$), -7.631 MeV (JISP16).

We used the 'Extrapolation A' described in the first chapter. The extrapolation technique is the same for every nucleus except ^{16}O and ^{16}N. For the interaction $NNLO_{opt}$, the selected $\hbar\Omega$ values are spaced by 2 MeV. For the JISP16 potential, the values were spaced by 2.5 MeV.

For the $A = 6$ nuclei, ^{6}He and ^{6}Li, the situation is similar. The relevant dependences are shown on figures 3.5, 1.4 and 3.6, 3.7. The extrapolated values of binding energies are within 3% of the experimental value and both potentials underbind the nucleus, $NNLO_{opt}$, again, more so. In [16] the values for the binding energy of ^{6}Li were calculated using NCSM with $N_{max} = 16$ and extrapolated using EFT-based extrapolation techniques. The value the authors obtained is $E_{gs} = 30.55(9)$ MeV for $NNLO_{opt}$ and $E_{gs} = 31.53(2)$ MeV for JISP16. We see that although our calculations were performed in a much smaller space, the final extrapolated agree with each other rather well.

Moving onto the $A = 8$ nuclei, we have studied the $J^\pi = 2^+$ ground state of ^{8}Li and the first excited $J^\pi = 2^+$ state of ^{8}Be. The maximum model space size we were able to achieve in this case is $N_{max} = 6$, which means that to use the 'Extrapolation A' technique, we had to use the value calculated in the very small $N_{max} = 0$ space, whose dimension is 17 for ^{8}Be, $J^\pi = 2^+$ and 9 for ^{8}Li, $J^\pi = 2^+$. This led to rather large extrapolation errors, which are one order higher than the errors calculated for $A = 6$ nuclei. Nevertheless, for the selected $A = 8$ systems, the SA-NCSM with both $NNLO_{opt}$ and JISP16 seems to overbind ^{8}Li, which is a rather loosely bound nucleus made of up 3 protons and 5 neutrons. On the other hand, it seems to predict the correct binding energies for the even-even nucleus ^{8}Be. The dependences of these nuclei on $(N_{max}, \hbar\Omega)$ are shown on figures 3.8, 3.9 and 3.10, 3.11.

Lastly, we have studied the ground state of ^{16}N and the ^{16}O first excited states, $J^\pi = 3^-$ and $J^\pi = 1^-$. The relevant $(\mathrm{N_{max}}, \hbar\Omega)$ dependences are shown on figures 3.12, 3.13, 3.14,3.15, 3.16 and 3.17. All of these states have negative parity. We have therefore, unlike in the previous positive parity calculations, used a model space defined by the sequence $N_{\max} = 1, 3, 5, 7...$, which describes negative parity states. Generally, we refer to a model space that coincides with the parity of the studied nucleus as 'natural' and as 'unnatural' when it does not. All of the calculations in this work were carried out in natural basis spaces. The maximum $\mathrm{N_{max}}$ value reached for these nuclei was $\mathrm{N_{max}} = 7$. Compared to the $\mathrm{N_{max}} = 6$ case of ^{8}Be, the basis space of ^{16}O, $J^\pi = 1^-$ is about 41 times larger (the dimensions are 4×10^5 and 1.6×10^7, respectively). The computations for $\mathrm{N_{max}} = 6, 7$ were carried out on the Frontera supercomputer [35].

In this case, we had to exclude the $\mathrm{N_{max}} = 0$ calculations from our extrapolations because the fits were too unstable and could not converge otherwise. The $\hbar\Omega$ values used for the extrapolation process also had to be spaced by 1 MeV in the case of the $\mathrm{NNLO_{opt}}$ interaction, since the calculations for $\mathrm{N_{max}} = 6, 7$ were performed in a smaller range. Apart from these differences, the extrapolation process was the same as for the other nuclei.

We have seen that for nuclei smaller than $A = 8$, both studied interactions predict very similar binding energies and the extrapolation errors are also quite similar. However, for both ^{16}N and ^{16}O, we observe large discrepancies between the two potentials. For the $J^\pi = 3^-$ excited state of ^{16}O, $\mathrm{NNLO_{opt}}$ overbinds the real value by about 27±5 MeV. The JISP16 overbinds the same state by about 7±2 MeV but offers much faster convergence and much smaller extrapolation errors. The situation is the same for the state $J^\pi = 1^-$, both potentials overbind the nucleus. Moreover, the $\mathrm{NNLO_{opt}}$ potential predicts wrong ordering of the states. While it is not apparent from the extrapolated values due to errors, the variational minimum of ^{16}O, $J^\pi = 3^-$ and ^{16}O, $J^\pi = 1^-$ are calculated as -117.833 MeV and -114.282 MeV, respectively, with the JISP16 potential, which therefore seems to predict the correct order of the states. It is worth noting, however, that we are still working within a rather small model space and it is not unthinkable that for larger values of $\mathrm{N_{max}}$, the energies would converge to the correct order even with the $\mathrm{NNLO_{opt}}$ potential.

The binding energies were extrapolated using only three successive values and, in the case of the $\mathrm{NNLO_{opt}}$ interaction, a smaller range of $\hbar\Omega$ values was used. Due to these facts, the extrapolation errors for this interaction especially are quite large. It is therefore very diffucult to draw any concrete conclusions about the $\mathrm{NNLO_{opt}}$ interaction and, ideally, calculations in larger model spaces would be needed to obtain better results.

Our calculations are summed up in table 3.1.

Table 3.1: Extrapolated binding energies obtained with the SA-NCSM and 'Extrapolation A' method compared to experimental values. All values in MeV. The source of experimental values is [36],[37].

Nucleus, J^π	E (JISP16)	E ($\mathrm{NNLO_{opt}}$)	E (exp.)	$\mathrm{N_{max}}$
^{3}He, $1/2^+$	7.66(1)	7.44(2)	7.716	12
^{3}H, $1/2^+$	8.37(1)	8.19(5)	8.481	12
^{6}Li, 1^+	30.7(3)	30.3(3)	31.993	8
^{6}He, 0^+	28.0(5)	27.2(4)	29.271	8
^{8}Li, 2^+	43(3)	45(6)	41.277	8
^{8}Be, 2^+	55(4)	53.0(2.5)	53.469	6
^{16}N, 2^-	129(4)	150(12)	117.97	6
^{16}O, 1^-	132(4)	168(14)	120.502	7
^{16}O, 3^-	132(3)	152(11)	121.489	7

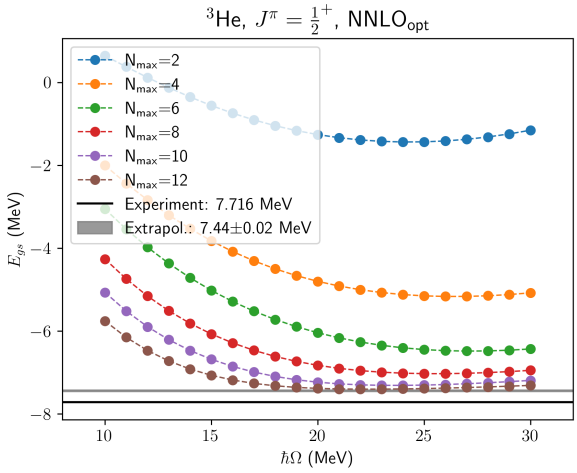

Figure 3.1: Convergence of the ground state binding energy of ^{3}He and the extrapolated value, calculated with the $\mathrm{NNLO_{opt}}$ potential

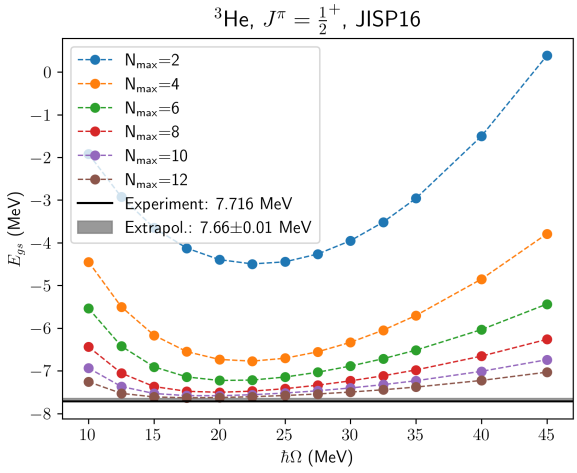

Figure 3.2: Convergence of the ground state binding energy of ^{3}He and the extrapolated value, calculated with the JISP16 potential

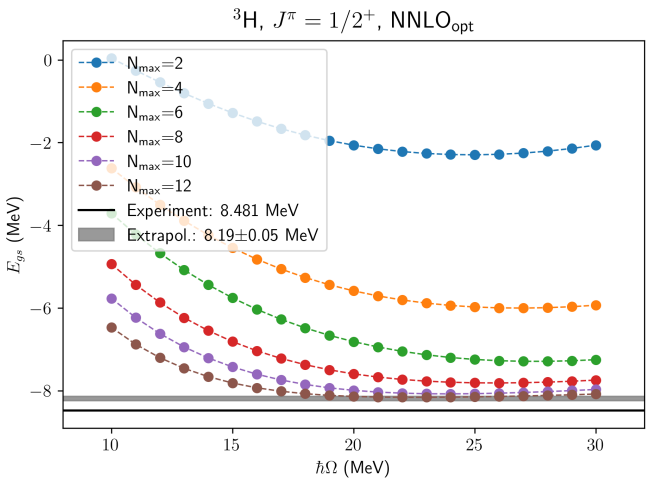

Figure 3.3: Convergence of the ground state binding energy of ^{3}H and the extrapolated value, calculated with the NNLO$_{\text{opt}}$ potential

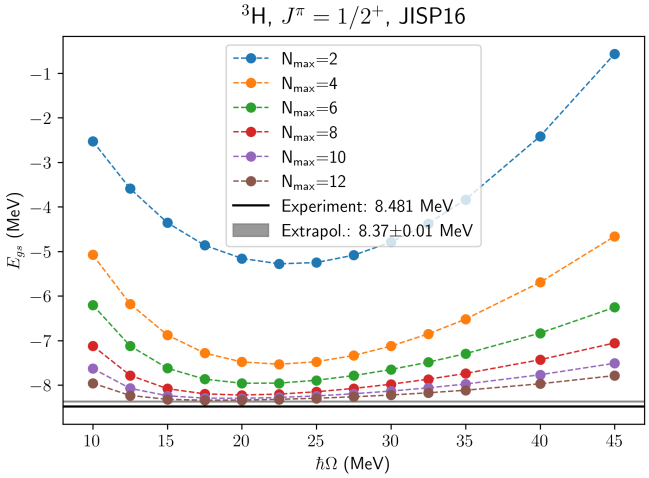

Figure 3.4: Convergence of the ground state binding energy of ^{3}H and the extrapolated value, calculated with the JISP16 potential

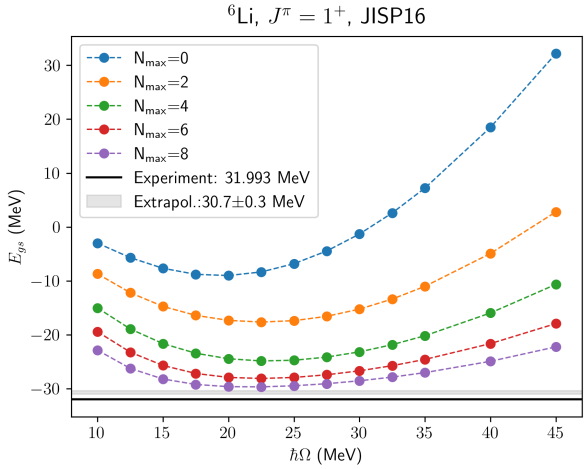

Figure 3.5: Convergence of the ground state binding energy of ^{6}Li and the extrapolated value, calculated with the JISP16 potential

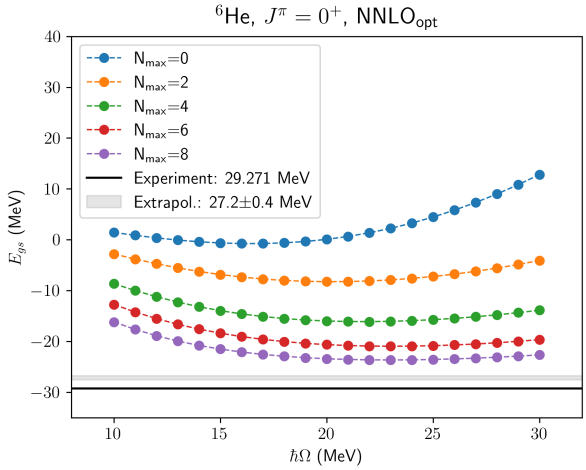

Figure 3.6: Convergence of the ground state binding energy of ^{6}He and the extrapolated value, calculated with the NNLO$_{\text{opt}}$ potential

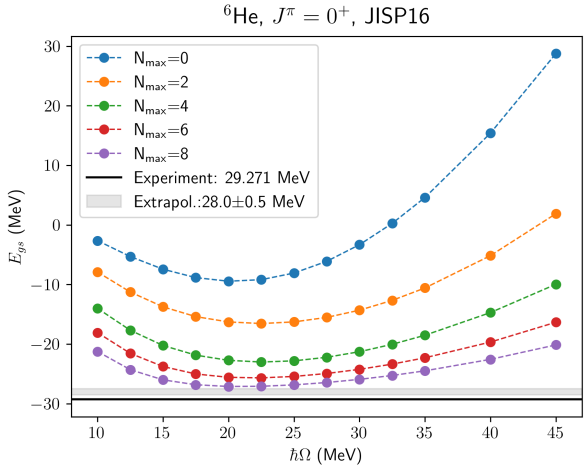

Figure 3.7: Convergence of the ground state binding energy of ^{6}He and the extrapolated value, calculated with the JISP16 potential

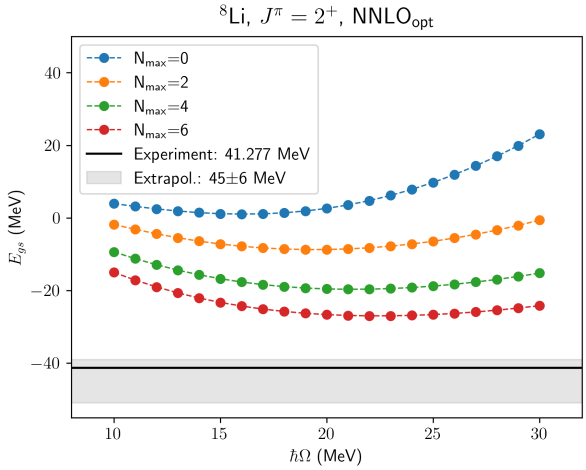

Figure 3.8: Convergence of the ground state binding energy of ^{8}Li and the extrapolated value, calculated with the NNLO$_{\text{opt}}$ potential

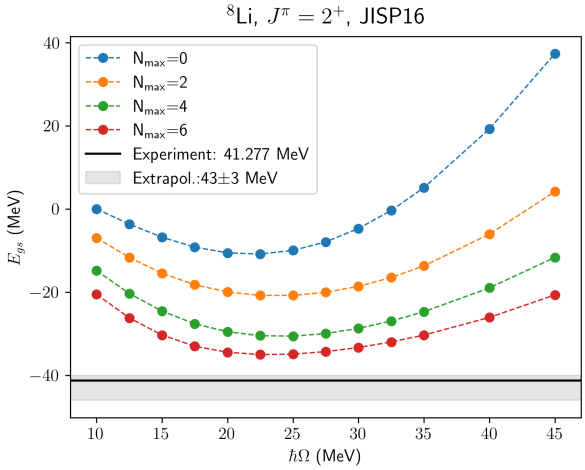

Figure 3.9: Convergence of the ground state binding energy of ^{8}Li and the extrapolated value, calculated with the JISP16 potential

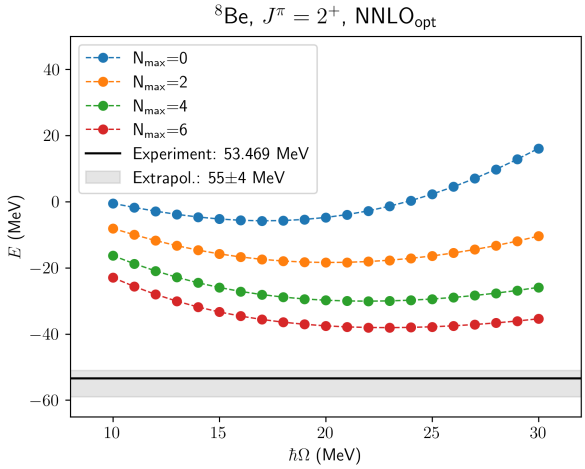

Figure 3.10: Convergence of the binding energy of ^{8}Be, $J^\pi = 2^+$ and the extrapolated value, calculated with the NNLO$_{\text{opt}}$ potential

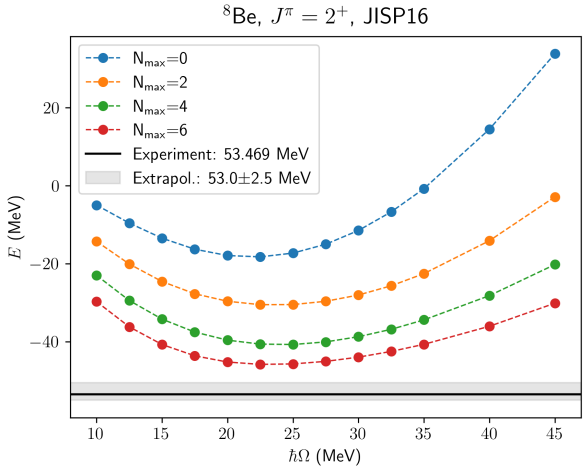

Figure 3.11: Convergence of the binding energy of ^{8}Be, $J^\pi = 2^+$ and the extrapolated value, calculated with the JISP16 potential

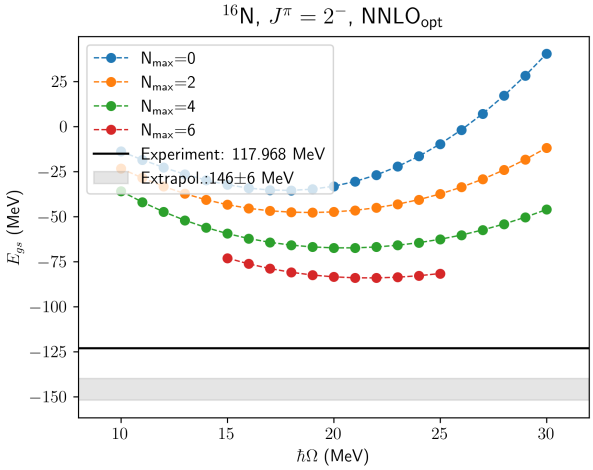

Figure 3.12: Convergence of the binding energy of ^{16}N, $J^\pi = 2^-$ and the extrapolated value, calculated with the NNLO$_{\text{opt}}$ potential

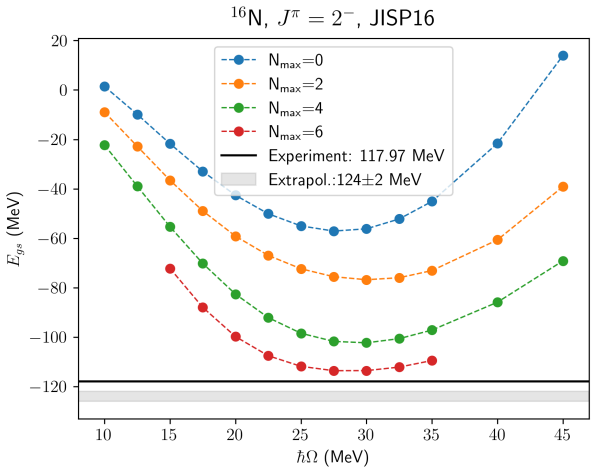

Figure 3.13: Convergence of the binding energy of ^{16}N, $J^\pi = 2^-$ and the extrapolated value, calculated with the JISP16 potential

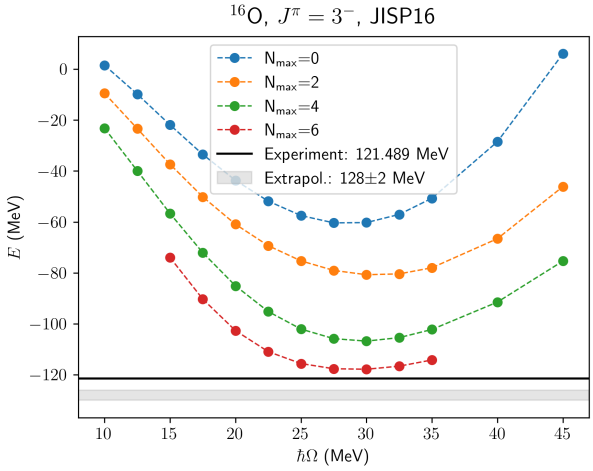

Figure 3.14: Convergence of the binding energy of ^{16}O, $J^\pi = 3^-$ and the extrapolated value, calculated with the JISP16 potential

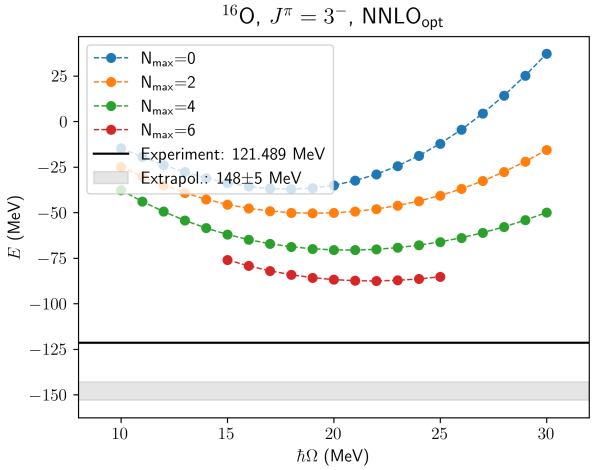

Figure 3.15: Convergence of the binding energy of ^{16}O, $J^\pi = 3^-$ and the extrapolated value, calculated with the NNLO$_{\text{opt}}$ potential

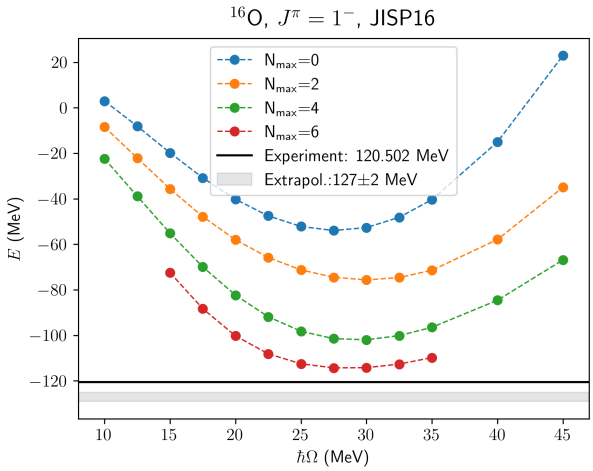

Figure 3.16: Convergence of the binding energy of ^{16}O, $J^\pi = 1^-$ and the extrapolated value, calculated with the JISP16 potential

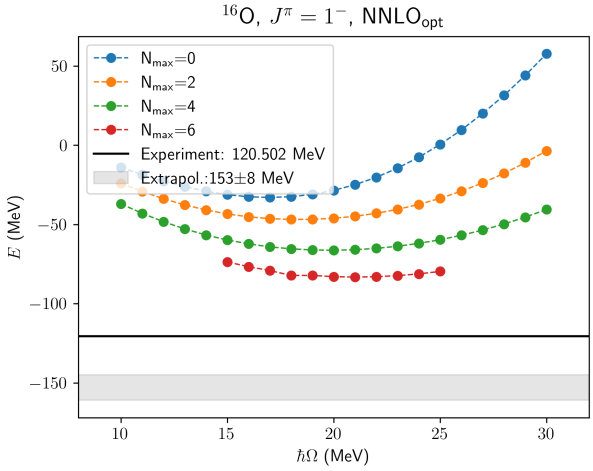

Figure 3.17: Convergence of the binding energy of ^{16}O, $J^\pi = 1^-$ and the extrapolated value, calculated with the NNLO$_{\text{opt}}$ potential

3.2 Low-lying spectrum of ^{16}N

According to experimental data, the nucleus ^{16}N has three low-lying excited states that are separated by energies of only a little over 100 keV. We carried out an SA-NCSM calculation of these states with model space defined by $N_{max} = 4$. While it cannot be expected that the excitation energies would converge close to the experimental value, we are interested if the interactions predict correct ordering of the states. The figure 3.18 shows the dependence of the spectrum calculated with the NNLO$_{opt}$ on $\hbar\Omega$. The ordering of the states is dependant on $\hbar\Omega$, but at none of the values does it agree with the experimental data. Just as we stated for the case of ^{16}O, the order of levels can change with increased model space size. The case of the spectrum calculated with the JISP16 interaction is similar, Fig. 3.19.

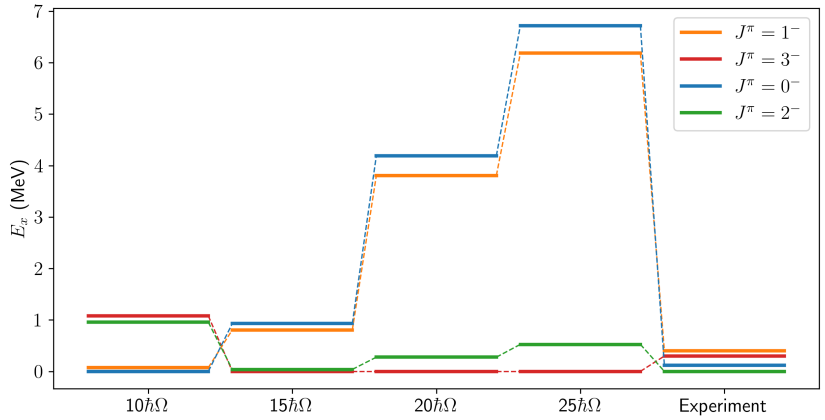

Figure 3.18: Dependence of the low-lying spectrum of ^{16}N on $\hbar\Omega$ calculated with the SA-NCSM and the NNLO$_{opt}$ interaction. Source of experimental data is [37].

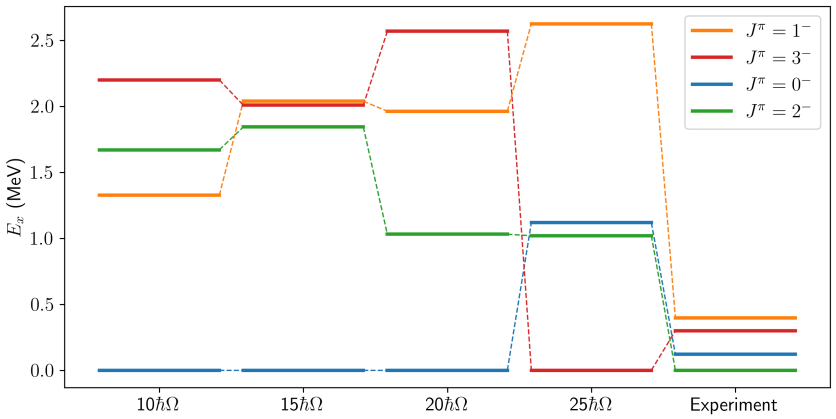

Figure 3.19: Dependence of the low-lying spectrum of ^{16}N on $\hbar\Omega$ calculated with the SA-NCSM and the JISP16 interaction. Source of experimental data is [37].

3.3 Beta Decay Matrix Elements

One of the problems of nuclear physics is the origin of the so-called 'quenching' of the coupling constant g_A. Compared to free neutron decay, its value usually needs to be quenched by a factor of about 0.75 to reproduce the correct experimental data of nuclear β-decay. In other words - the value of the matrix element M_{GT} is, in reality, smaller than theory predicts. Currently, the most advanced ab initio calculations studying GT transitions in nuclei were performed in [38], where the quenching is attributed to corrections of the GT operator that arise due to two-body currents and to missing correlations in the wavefunctions. In this section, we will present our results of the M_{GT} matrix elements calculated with the SA-NCSM and the $\mathrm{NNLO_{opt}}$, JISP16 interactions and compare them to experimental data [39].

3.3.1 Convergence of the Gamow-Teller Operator

We have obtained an excellent agreement with experiment for the case of ^{3}H β-decay with the $\mathrm{NNLO_{opt}}$ interaction. The calculation performed in the $\mathrm{N_{max}}$= 12 model space seems to be almost fully converged. We have therefore estimated the final value as 2.318(12), where the spread due to the small dependence on $\hbar\Omega$ was taken as the error. We estimate the final value for the JISP16 potential as 2.339(14). Both values are slightly above the experimental value of 2.317(4). The dependences of the GT operator on ($\mathrm{N_{max}}$,$\hbar\Omega$) for tritium decay are shown on figures 3.20 and 3.21.

The GT transition operator between the heavier, $A = 6$ nuclei is not well converged in the $\mathrm{N_{max}}$= 8 model space, as can be seen on figures 3.22 and 3.23. However, notice the scale on the left. The GT operator converges very fast and the values obtained even in the small $\mathrm{N_{max}}$= 2 model space are numerically very close to the much larger $\mathrm{N_{max}}$= 8 and the experimental value. We again estimate the final value as the minimum obtained with the largest model space and the error as the spread due to the dependence on $\hbar\Omega$. We obtain 2.26(7) for $\mathrm{NNLO_{opt}}$ and 2.23(6) for JISP16. The experimental value is 2.174(3). We see that even without considering any quenching, the SA-NCSM predicts values that are very close to the experimental ones. The dependences of the GT operator on ($\mathrm{N_{max}}$,$\hbar\Omega$) are generally complicated and cannot by extrapolated like the binding energies since they do not converge exponentially.

Next, we studied the transition from the ground state of ^{8}Li to the $J^\pi = 2^+$ first excited state of ^{8}Be. The relevant dependences are shown on figures 3.24 and 3.25. In this case, the results are not converged and calculations within larger model spaces would have to be made to obtain better results. Nevertheless, we observe that the curves in ($\mathrm{N_{max}}$, $\hbar\Omega$) seem to converge for the few smallest $\hbar\Omega$ values. This is usually a good indicator of the final value, as can be seen from, e.g., the decay of ^{6}He calculated with the JISP16 potential, where the values at $\hbar\Omega$ =40 to 45 MeV seem to be constant with the increasing $\mathrm{N_{max}}$. From this, it can be estimated that for the $\mathrm{NNLO_{opt}}$ interactions, the M_{GT} of the ^{8}Be decay is around 0.2 and is below the experiment. For JISP16, the converged value seems to be above the experimental value, but it cannot be estimated.

Lastly, we have attempted to calculate the beta decay of the ground state

of ^{16}N into the negative parity states of ^{16}O, $J^\pi = 1^-$ and $J^\pi = 3^-$ (scheme of the ^{16}N β-decay is shown on Fig. 3.31). The relevant dependences are shown on figures 3.26, 3.27 and 3.28 3.29. The matrix elements are not well converged within the N_{max}=7 model space and are impossible to extrapolate due to the complicated dependences on $\hbar\Omega$. The GT matrix element of ^{16}N$\rightarrow^{16}$O, $J^\pi = 1^-$ calculated with the NNLO$_{opt}$ seems to converge to the value of around 0.32, which is slightly below the experimental value. The same transition, but calculated with the JISP16 interaction does not seem to be converged at all.

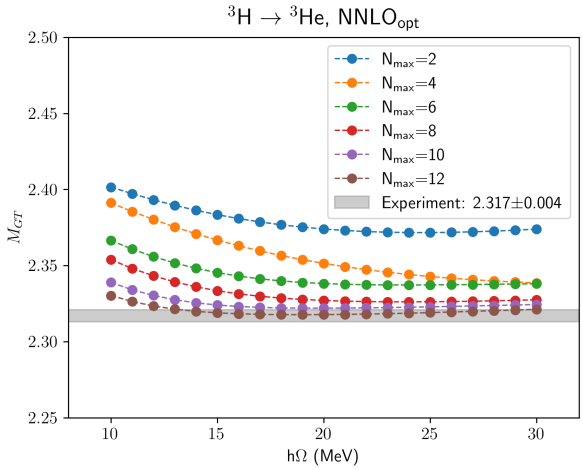

Figure 3.20: GT transition between the ground states of ^{3}H and ^{3}He calculated with the SA-NCSM and the NNLO$_{opt}$ interaction. The shaded area represents the experimental value and its error.

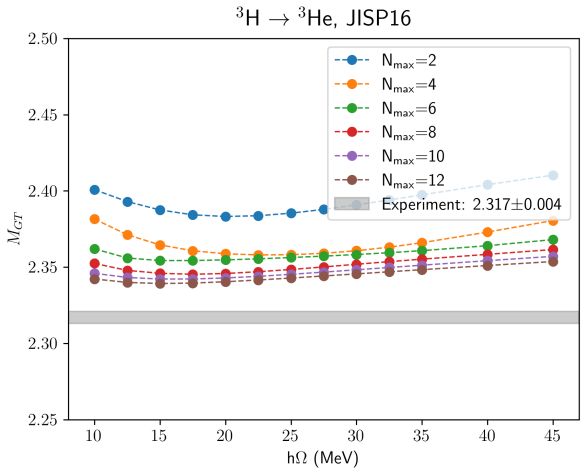

Figure 3.21: GT transition between the ground states of ^{3}H and ^{3}He calculated with the SA-NCSM and the JISP16 interaction. The shaded area represents the experimental value and its error.

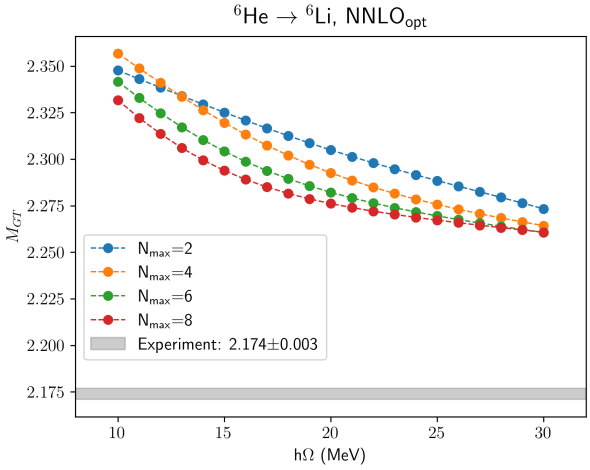

Figure 3.22: GT transition between the ground states of ^{6}He and ^{6}Li calculated with the SA-NCSM and the NNLO$_{opt}$ interaction. The shaded area represents the experimental value and its error.

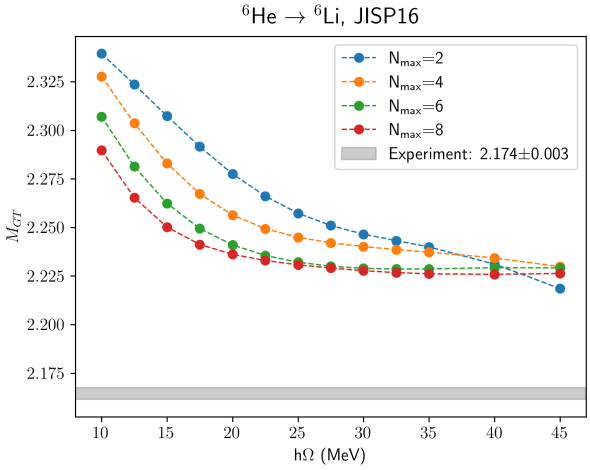

Figure 3.23: GT transition between the ground states of ^{6}He and ^{6}Li calculated with the SA-NCSM and the JISP16 interaction. The shaded area represents the experimental value and its error.

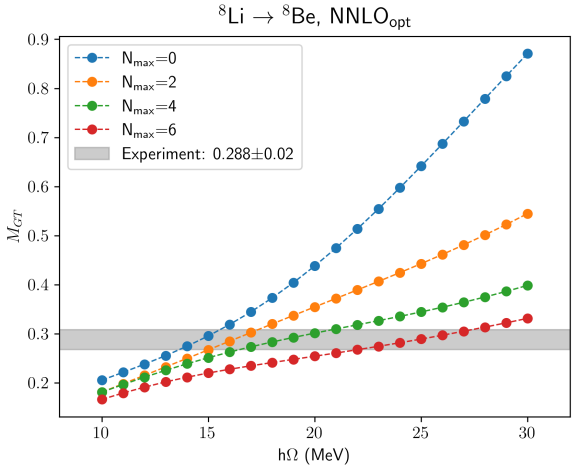

Figure 3.24: GT transition between the ground state of ^{8}Li and the $J^\pi = 2^+$ state of ^{8}Be calculated with the SA-NCSM and the NNLO$_{\text{opt}}$ interaction. The shaded area represents the experimental value and its error.

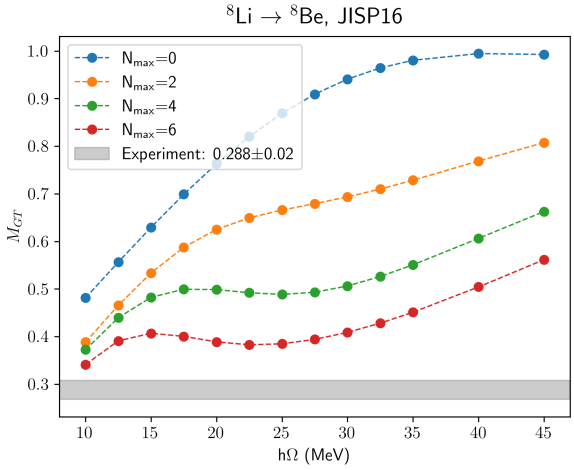

Figure 3.25: GT transition between the ground state of ^{8}Li and the $J^\pi = 2^+$ state of ^{8}Be calculated with the SA-NCSM and the JISP16 interaction. The shaded area represents the experimental value and its error.

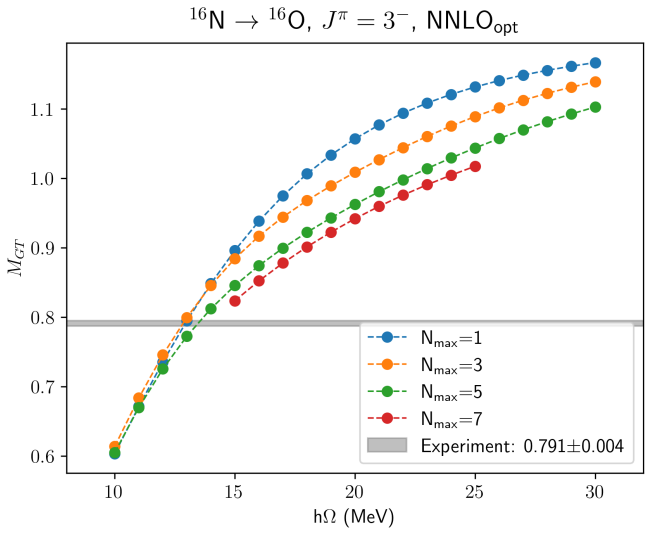

Figure 3.26: GT transition between the ground state of ^{16}N and the $J^\pi = 3^-$ excited state of ^{16}O calculated with the SA-NCSM and the NNLO$_{opt}$ interaction. The shaded area represents the experimental value and its error.

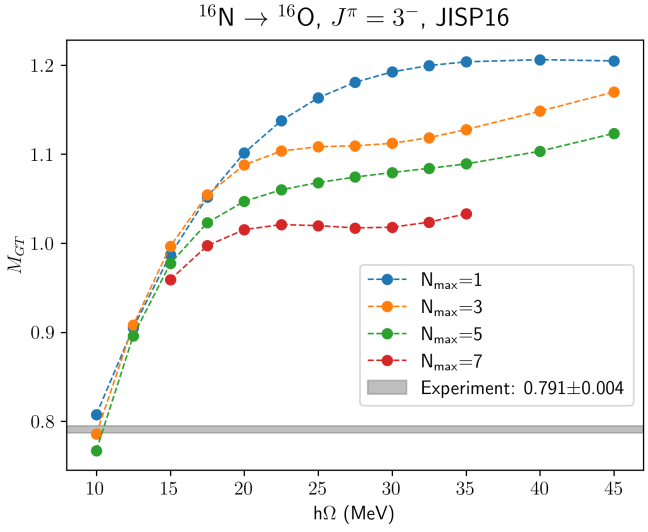

Figure 3.27: GT transition between between the ground state of ^{16}N and the $J^\pi = 3^-$ excited state of ^{16}O calculated with the SA-NCSM and the JISP16 interaction. The shaded area represents the experimental value and its error.

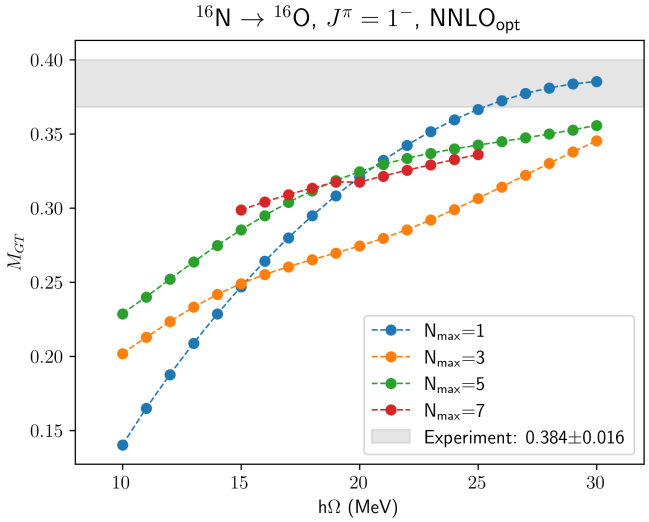

Figure 3.28: GT transition between between the ground state of ^{16}N and the $J^\pi = 1^-$ excited state of ^{16}Ocalculated with the SA-NCSM and the NNLO$_{\text{opt}}$ interaction. The shaded area represents the experimental value and its error.

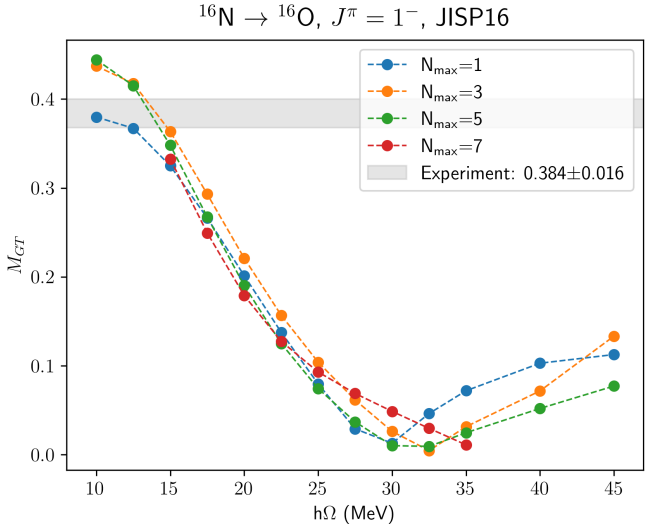

Figure 3.29: GT transition between between the ground state of ^{16}N and the $J^\pi = 1^-$ excited state of ^{16}O calculated with the SA-NCSM and the JISP16 interaction. The shaded area represents the experimental value and its error.

3.3.2 Beta Decay in the SA-NCSM

As was already stated in section 2.1.4, neither the Gamow-Teller operator nor the Fermi operator can change the λ and μ labels of an SU(3) basis state. We would then expect that the dominant SU(3) irreps describing the state of the parent nucleus will be dominant also in the model space of the daughter nucleus, except their total spin should differ by one for a $\Delta S = 1$ transition.

The β^- decay of ^{6}He, $J^\pi = 0^+$ is rather simple, with only one possible final state - ^{6}Li, $J^\pi = 0^+$ [40]. Figure 3.30 compares the dominant SU(3)⊗SU(2) irreps $(S_p, S_n, S)\lambda\,\mu$ of these nuclei in the subspaces $N\hbar\Omega = 0, 2, 4\hbar\Omega$ and 6. We see that in each subspace, the SU(3) labels λ, μ of the parent nucleus correspond perfectly to those of the daughter nucleus. Also, notice that the leading irrep in each successive subspace is given by the formula 1.4.31.

Figure 3.31 shows the decay scheme of ^{16}N, which has many final states of which we have studied only the allowed transitions into $J^\pi = 1^-$ and 2^- levels of ^{16}O. Their wavefunctions are compared in Figure 3.32. In this case, we do not find one-to-one correspondence of the most dominant basis states. For example, the SU(3) irrep $(\lambda\,\mu) = (1\,0)$ is with 15.8% the second most dominant basis state of $^{16}N^{2-}$ but the highest probable irrep with the same labels has an amplitude around 10^{-6} in the wavefunctions of both of the daughter nuclei. The situation is similar for the decay of ^{8}Li (Fig. 3.33). This decay has only one final state, ^{8}Be, $J^\pi = 2^+$ [41]. We again observe only partial correspondence of the basis spaces.

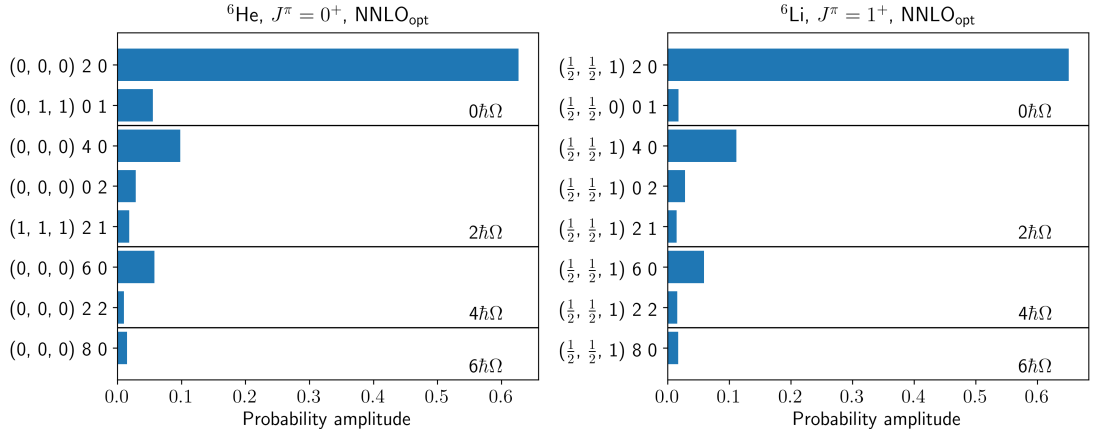

Figure 3.30: Comparison of the dominant irreps in wavefunctions of the ground states of ^{6}He and ^{6}Li calculated with the NNLO$_{opt}$ interaction and $\hbar\Omega = 20$ MeV, N_{max}=8. Only irreps with amplitude larger than ∼1% are shown.

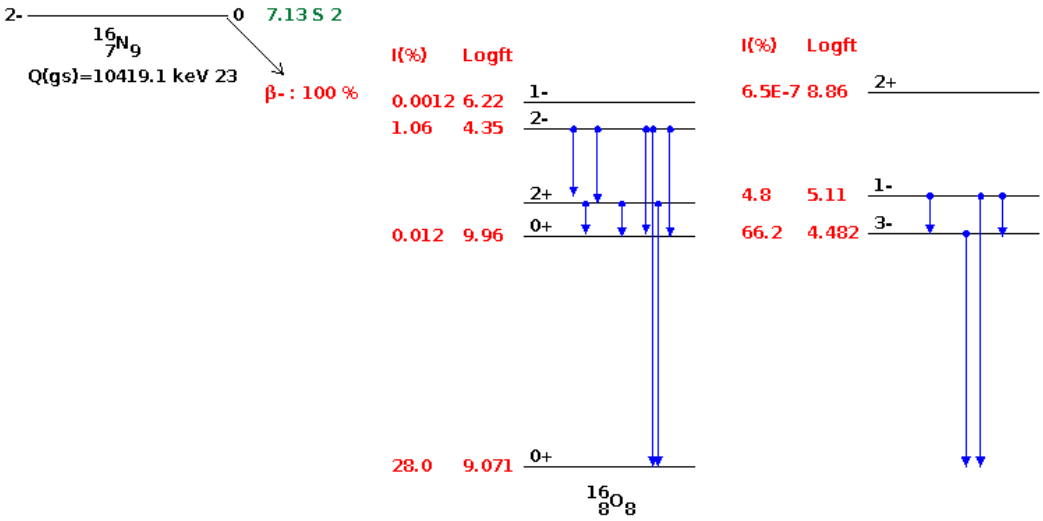

Figure 3.31: Scheme of the $^{16}\mathrm{N}^{2-}$ β decay. Source of the data is [37].

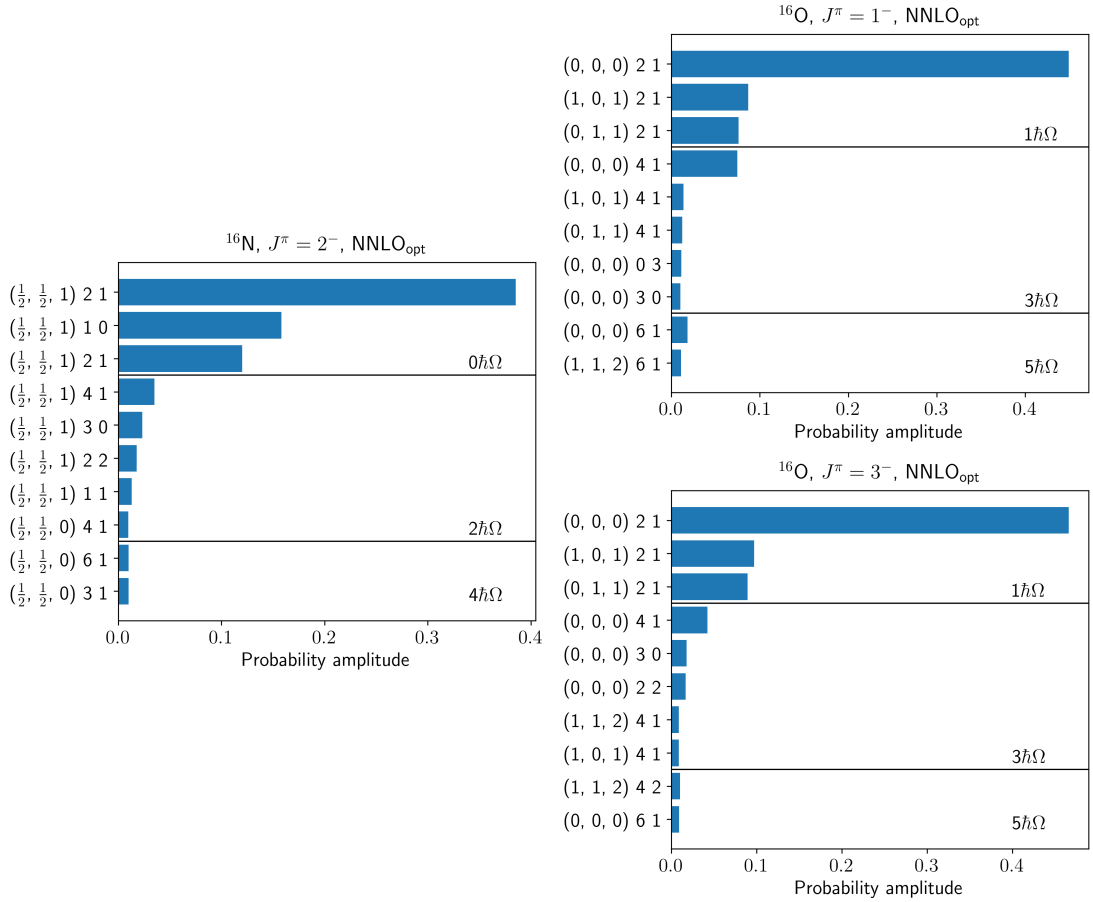

Figure 3.32: Comparison of the dominant irreps in wavefunctions of the ground state of ^{16}N and its decay products ^{16}O, $J^\pi = 1^-, 3^-$ calculated with the NNLO$_{\mathrm{opt}}$ interaction and $\hbar\Omega = 20$ MeV, N_{max}=6,7. Only irreps with amplitude larger than $\sim$1% are shown.

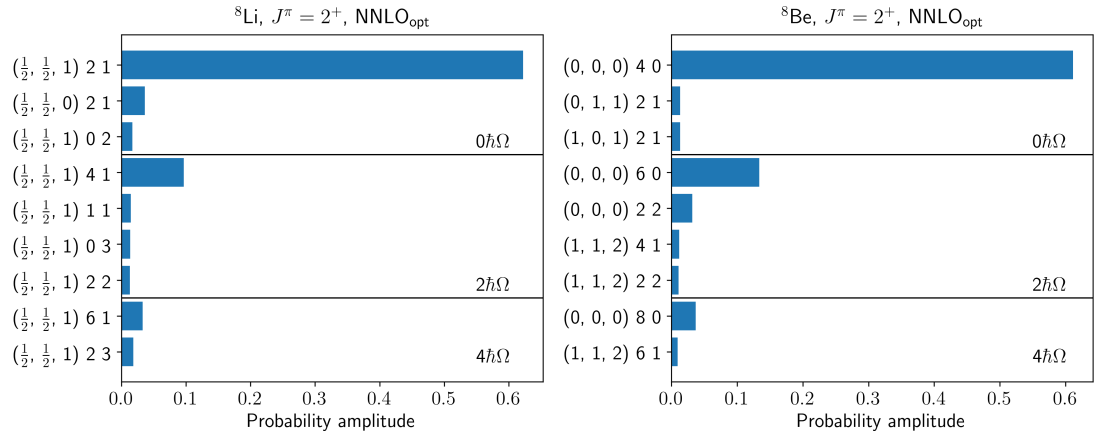

Figure 3.33: Comparison of the dominant irreps in wavefunctions of ^{8}Be, $J^\pi = 2^+$ and its daughter nucleus, the ground state of ^{8}Li, calculated with the NNLO$_{\text{opt}}$ interaction and $\hbar\Omega = 20$ MeV, N$_{\text{max}}$=6. Only irreps with amplitude larger than $\sim$1% are shown.

3.3.3 Beta Decay Matrix Elements in Truncated Model Spaces

One of the biggest advantages of the SA-NCSM is the fact that we can include only a few irreps with large probability amplitudes in our model space but still obtain convergence close to the full model space while drastically reducing the dimension of the basis. In [8], it is shown that this approach is applicable when calculating quadrupole momenta, $B(E2)$ transition probabilities, nuclear radii, etc. We are interested in the behavior of the GT operator in truncated model spaces.

For convenience, we will first work with the small N$_{\text{max}}$=2 model spaces of ^{6}He and ^{6}Li. We define a parameter ε as the fraction of the model space used (i.e., ε=0 is equivalent to the full N$_{\text{max}}$=0 and $\varepsilon = 1$ to the full N$_{\text{max}}$=2 space). We have to truncate both the model space of the parent and daughter nucleus; hence ε will be defined as the sum of dimensions of the truncated model spaces of both nuclei. Figure 3.34 shows the values of M_{GT} (left) and binding energy E (right) as functions of ε. The model spaces were truncated by selecting the most dominant spin triplets first and then adding the rest in accordance with their decreasing probability amplitude. The binding energy converges as expected - including the least probable states has only a very small impact on the resulting value. Unlike the binding energy, the value of the Gammow-Teller reduced matrix element is highly dependent even on states with low probability amplitudes and its convergence is not monotonous. This would then suggest that the usual truncation schemes of the SA-NCSM cannot be used in this case.

We have also performed similar calculations for the transition ^{16}N$\rightarrow^{16}$O, $J^\pi = 3^-$ which are shown in Figure 3.35. This time, the model spaces were truncated by first selecting individual SU(3)$\otimes$SU(2) irreps and later by including whole spin triplets. The individual irreps were selected in such a way, that they conform to the selection rules of the GT operator, i.e., only irreps with the same SU(3) labels and $\Delta S = 1$ were selected. For any other selection, the matrix elements are

trivially zero. The consequence of this is that the binding energy of ^{16}N on the left side of the figure 3.35 converges slower than it could, because the irreps were not necessarily chosen by their decreasing probability amplitude. Again, unlike the binding energy, the Gamow-Teller operator changes its value significantly by including even one irrep and there does not seem to be any meaningful way in which the value calculated in a truncated model space can be related to that of a full model space. We have also carried out similar calculations with the JISP16 interaction and different values $\hbar\Omega$. This had, however, no impact on the convergence of the GT operator and obtained dependences on ε were practically the same as the ones showed in figures 3.34 and 3.35.

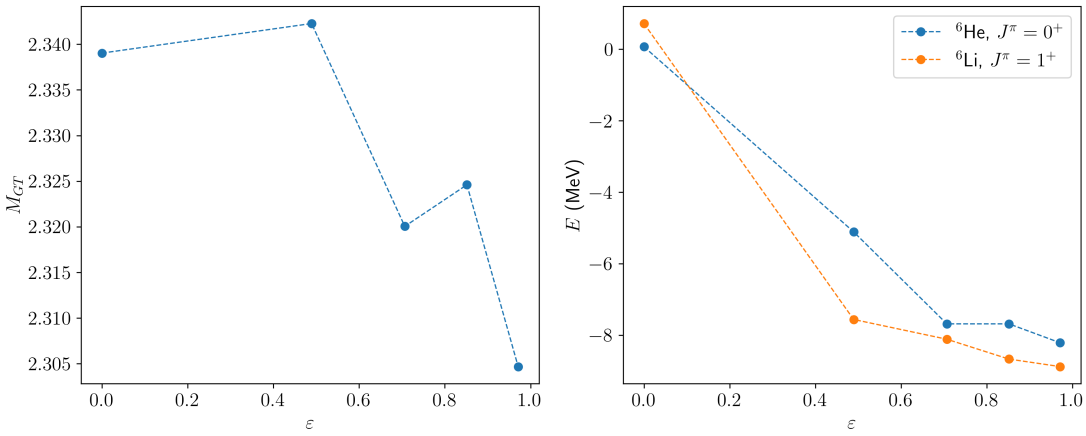

Figure 3.34: Left: Convergence of the GT operator between ^{6}He, $J^\pi = 0^+$ and ^{6}Li, $J^\pi = 1^+$ in the $\langle N^\perp_{\max}\rangle N^\top_{\max} = \langle 0\rangle 2$ space. Right: Convergence of the binding energies of ^{6}He, $J^\pi = 0^+$ and ^{6}Li, $J^\pi = 0^+$ in the $\langle N^\perp_{\max}\rangle N^\top_{\max} = \langle 0\rangle 2$ subspace. Both: Calculated with the NNLO$_{\text{opt}}$ potential and $\hbar\Omega$=20 MeV

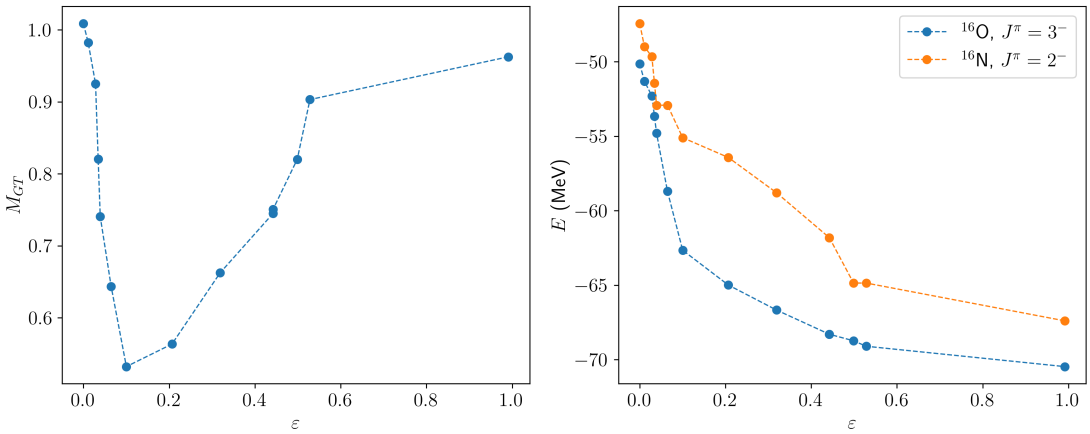

Figure 3.35: Left: Convergence of the GT operator between ^{16}N, $J^\pi = 2-$ and ^{16}O, $J^\pi = 3^-$ in the $\langle N^\perp_{\max}\rangle N^\top_{\max} = \langle 3\rangle 5$ space. Right: Convergence of the binding energies of ^{16}N, $J^\pi = 2-$ and ^{16}O, $J^\pi = 3^-$ in the $\langle N^\perp_{\max}\rangle N^\top_{\max} = \langle 3\rangle 5$ space. Both: Calculated with the NNLO$_{\text{opt}}$ potential and $\hbar\Omega$=20 MeV

Conclusion

We have studied the binding energies and Gamow-Teller transition matrix elements of various nuclei with masses $A \leq 16$ within the framework of the symmetry adapted no-core shell model. Except for the lightest $A = 3$ nuclei, the binding energies were not well converged in the model spaces used and extrapolation techniques had to be employed. The extrapolated binding energies of $A = 8$ and lighter nuclei are in good agreement with the experiment and both employed interactions, $\mathrm{NNLO_{opt}}$ and JISP16, predict very similar values. Based on the extrapolated values, both potentials seem to overbind the heavier nuclei, ^{16}O and ^{16}N. The JISP16 interaction by about 8 MeV and $\mathrm{NNLO_{opt}}$ by about 30 to 40 MeV. However, due to the larger extrapolation errors, especially in the case of $\mathrm{NNLO_{opt}}$, it is impossible to draw any conclusions.

The Gamow-Teller operator matrix elements of the transitions $^3\mathrm{H} \to {}^3\mathrm{He}$ and $^6\mathrm{He} \to {}^6\mathrm{Li}$ converge very quickly and even values calculated in smaller model spaces, e.g., $\mathrm{N_{max}}$=4 or 6, give a very good estimate of the values calculated in larger model spaces. The values calculated with the SA-NCSM are in very good agreement with the experiment for both interactions. The convergence of the Gamow-Teller matrix elements of studied transitions between $A = 8$ and $A = 16$ nuclei is in comparison much slower. Unlike the case of binding energies, extrapolation techniques could not be used due to the irregular dependence on model space parameters. We were not able to obtain a final value for these transitions, calculations in larger model spaces would be needed. Especially, the behaviour of the transition matrix elements between negative parity ^{16}N and ^{16}O states has proven to be very problematic. We have observed that the Gamow-Teller operator is rather sensitive to different interactions, as can be seen in the case of the $^{16}\mathrm{N} \to {}^{16}\mathrm{O}$, $J^\pi = 1^-$ transition, where we have obtained very different dependences on the model space parameters for the two potentials, $\mathrm{NNLO_{opt}}$ and JISP16.

We have tried to apply the SA-NCSM truncation process to the calculations of the Gamow-Teller operator. We have observed that this operator is highly dependent even on irreps that have very low probability amplitudes in the respective wavefunctions. No reliable way to calculate this operator in model spaces truncated by selecting SU(3)⊗SU(2) irreps has been found. This would suggest that for the calculation of the Gamow-Teller matrix elements, we cannot use the main advantage of the SA-NCSM and we have to consider only complete $\mathrm{N_{max}}$ model spaces. That greatly limits the number of nuclei we are able to reach with reasonable demands on computational resources.

Bibliography

[1] J. P. Elliott and John Douglas Cockcroft. Collective motion in the nuclear shell model. i. classification schemes for states of mixed configurations. *Proceedings of the Royal Society of London. Series A. Mathematical and Physical Sciences*, 245(1240):128–145, 1958.

[2] Maria Goeppert Mayer. On closed shells in nuclei. ii. *Phys. Rev.*, 75, Jun 1949.

[3] K. L. G. Heyde. *The Nuclear Shell Model*. Second Corrected and Enlarged Edition. Springer-Verlag, Heidelberg, Germany, 1994.

[4] J. Suhonen. *From Nucleons to Nucleus: Concepts of Microscopic Nuclear Theory*. Springer, 2007.

[5] V. Zelevinsky and A. Volya. *Physics of Atomic Nuclei*. Wiley-VCH, Weinheim, Germany, 2017.

[6] Heiko Hergert. A guided tour of ab initio nuclear many-body theory. *Frontiers in Physics*, 8, October 2020.

[7] Bruce R. Barrett, Petr Navratil, and James P. Vary. Ab initio no core shell model. *Progress in Particle and Nuclear Physics*, 69:131–181, March 2013.

[8] Kristina D. Launey, Tomas Dytrych, and Jerry P. Draayer. Symmetry-guided large-scale shell-model theory. *Progress in Particle and Nuclear Physics*, 89:101–136, July 2016.

[9] Cornelius Lanczos. An iteration method for the solution of the eigenvalue problem of linear differential and integral operators. *Journal of research of the National Bureau of Standards*, 45:255–282, 1950.

[10] R. R. Whitehead, A. Watt, B. J. Cole, and I. Morrison. *Computational Methods for Shell-Model Calculations*, pages 123–176. Springer US, Boston, MA, 1977.

[11] P. K. Rath, A. Faessler, H. Muther, and A. Watt. A practical solution to the problem of spurious states in shell-model calculations. *Journal of Physics G: Nuclear and Particle Physics*, 16(2):245, February 1990.

[12] D.H. Gloeckner and R.D. Lawson. Spurious center-of-mass motion. *Physics Letters B*, 53(4):313–318, 1974.

[13] A. Ekström, G. Baardsen, C. Forssé n, G. Hagen, M. Hjorth-Jensen, G. R. Jansen, R. Machleidt, W. Nazarewicz, T. Papenbrock, J. Sarich, and S. M. Wild. Optimized chiral nucleon-nucleon interaction at next-to-next-to-leading order. *Physical Review Letters*, 110(19), may 2013.

[14] A.M. Shirokov, J.P. Vary, A.I. Mazur, and T.A. Weber. Realistic nuclear hamiltonian: Ab exitu approach. *Physics Letters B*, 644(1):33–37, 2007.

[15] P. Maris, J. P. Vary, and A. M. Shirokov. Ab initio no-core full configuration calculations of light nuclei. *Physical Review C*, 79(1), January 2009.

[16] Ik Jae Shin, Youngman Kim, Pieter Maris, James P Vary, Christian Forssén, Jimmy Rotureau, and Nicolas Michel. Ab initio no-core solutions for 6li. *Journal of Physics G: Nuclear and Particle Physics*, 44(7):075103, May 2017.

[17] M. Harvey. *Advances in Nuclear Physics: Volume 1 - The Nuclear SU3 Model*, pages 67–182. Springer US, Boston, MA, 1968.

[18] A Arima. Elliott's su(3) model and its developments in nuclear physics. *Journal of Physics G: Nuclear and Particle Physics*, 25(4):581, apr 1999.

[19] J.P. Draayer and S.A. Williams. Coupling coefficients and matrix elements of arbitrary tensors in the elliott projected angular momentum basis. *Nuclear Physics A*, 129(3):647–665, 1969.

[20] A. Bohr and B.R. Mottelson. *Nuclear Structure*. Number sv. 1 in Nuclear Structure. World Scientific, 1998.

[21] Pavel Cejnar, Jan Jolie, and Richard F. Casten. Quantum phase transitions in the shapes of atomic nuclei. *Rev. Mod. Phys.*, 82:2155–2212, Aug 2010.

[22] Richard F. Casten, et al. *Algebraic Approaches to Nuclear Structure*. Springer US, Boston, MA, 1992.

[23] Grigor Sargsyan. Electromagnetic transitions and beta decays in nuclei from the ab initio symmetry-adapted no-core shell model. *LSU Doctoral Dissertations.*, 2021.

[24] T. Dytrych, K. D. Launey, J. P. Draayer, P. Maris, J. P. Vary, E. Saule, U. Catalyurek, M. Sosonkina, D. Langr, and M. A. Caprio. Collective modes in light nuclei from first principles. *Phys. Rev. Lett.*, 111:252501, Dec 2013.

[25] V. K. Khersonskii D. A. Varshalovich, A. N. Moskalev. *Quantum Theory of Angular Momentum*. World Scientific, Singapore, 1988.

[26] Tomas Dytrych. Private communication.

[27] Tomas Dytrych, Daniel Langr, Jerry P. Draayer, Kristina D. Launey, and Daniel Gazda. Su3lib: A c++ library for accurate computation of wigner and racah coefficients of su(3). *Computer Physics Communications*, 269, DEC 2021.

[28] T. Dytrych. Lsu3shell code. *Louisiana State University, available under the GNU General Public License at the git repository, http://sourceforge.net/projects/lsu3shell*, 2013.

[29] C. S. Wu, E. Ambler, R. W. Hayward, D. D. Hoppes, and R. P. Hudson. Experimental test of parity conservation in beta decay. *Phys. Rev.*, 105:1413–1415, Feb 1957.

[30] Samuel S. M. Wong. *Introductory Nuclear Physics*, chapter 5, pages 161–204. John Wiley and Sons, Ltd, 1998.

[31] M. Brodeur et al. Nuclear β decay as a probe for physics beyond the Standard Model. *arXiv:nucl-ex/2301.03975*, Jan 2023.

[32] G. H. Sargsyan, K. D. Launey, M. T. Burkey, A. T. Gallant, N. D. Scielzo, G. Savard, A. Mercenne, T. Dytrych, D. Langr, L. Varriano, B. Longfellow, T. Y. Hirsh, and J. P. Draayer. Impact of clustering on the ^{8}Li β decay and recoil form factors. *Phys. Rev. Lett.*, 128:202503, May 2022.

[33] I S Towner and J C Hardy. The evaluation of vud and its impact on the unitarity of the cabibbo–kobayashi–maskawa quark-mixing matrix. *Reports on Progress in Physics*, 73(4):046301, mar 2010.

[34] P A Zyla, R M Barnett, J Beringer, O Dahl, D A Dwyer, D E Groom, C J Lin, K S Lugovsky, and E et al. Pianori. Review of Particle Physics. *Progress of Theoretical and Experimental Physics*, 2020(8), 08 2020. 083C01.

[35] Dan Stanzione, John West, R. Todd Evans, Tommy Minyard, Omar Ghattas, and Dhabaleswar K. Panda. Frontera: The evolution of leadership computing at the national science foundation. In *Practice and Experience in Advanced Research Computing*, PEARC '20, page 106–111, New York, NY, USA, 2020. Association for Computing Machinery.

[36] Meng Wang, W.J. Huang, F.G. Kondev, G. Audi, and S. Naimi. The ame 2020 atomic mass evaluation (ii). tables, graphs and references*. *Chinese Physics C*, 45(3):030003, mar 2021.

[37] D.R. Tilley, H.R. Weller, and C.M. Cheves. Energy levels of light nuclei a = 16–17. *Nuclear Physics A*, 564(1):1–183, 1993.

[38] P. Gysbers, G. Hagen, J. Holt, G. Jansen, T. Morris, P. Navrátil, T. Papenbrock, S. Quaglioni, A. Schwenk, S. Stroberg, and Klaus Wendt. Discrepancy between experimental and theoretical beta-decay rates resolved from first principles. *Nature Physics*, 15:1, 05 2019.

[39] W.-T. Chou, E. K. Warburton, and B. A. Brown. Gamow-teller beta-decay rates for a<18 nuclei. *Phys. Rev. C*, 47:163–177, Jan 1993.

[40] D.R. Tilley, C.M. Cheves, J.L. Godwin, G.M. Hale, H.M. Hofmann, J.H. Kelley, C.G. Sheu, and H.R. Weller. Energy levels of light nuclei a=5, 6, 7. *Nuclear Physics A*, 708(1):3–163, 2002.

[41] D.R. Tilley, J.H. Kelley, J.L. Godwin, D.J. Millener, J.E. Purcell, C.G. Sheu, and H.R. Weller. Energy levels of light nuclei a=8,9,10. *Nuclear Physics A*, 745(3):155–362, 2004.

List of Figures

List of Tables